Jarkko J. Saarinen

Nanophotonics on Paper Platform

Åbo Akademi University

Jarkko J. Saarinen

Born 1978

Previous studies and degrees

PhD, University of Joensuu, 2002

MSc, University of Joensuu, 2000

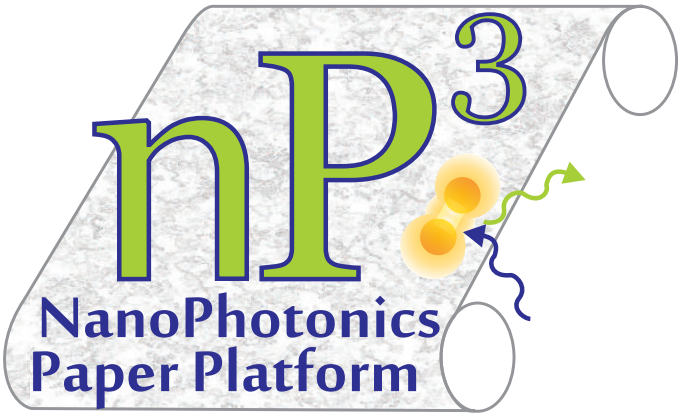

Nanophotonics on Paper Platform

Jarkko J. Saarinen

Academic Dissertation

Laboratory of Natural Materials Technology
Center for Functional Materials
Faculty of Science and Engineering
Åbo / Turku, Finland, 2020

Supervisor

Professor Martti Toivakka
Laboratory of Natural Materials Technology
Center for Functional Materials
Åbo Akademi, Åbo / Turku, Finland

Pre-examiners

Professor Patrick A. C. Gane
Department of Bioproducts and Biosystems
Aalto University
Espoo, Finland

and

Professor Hak Lae Lee
Department of Forest Sciences
College of Agriculture and Life Sciences
Seoul National University
Seoul, Korea

Opponent for the public defence

Professor Patrick A. C. Gane
Department of Bioproducts and Biosystems
Aalto University
Espoo, Finland

ISBN 978-952-12-3986-1

Painosalama Oy, Åbo / Turku 2020

Dedicated to Vilppu & Viola

– the Bright Light and Love of my life!

PREFACE

The research work for this thesis was carried during my ten year term at the Åbo Akademi University, Finland in 2008–2018. The first discussions for completing a second PhD degree in Technology were established already in 2009, and I find it very satisfying to see this piece of work finally completed.

There are several colleagues that I would like to acknowledge for the support during this work. First, the supervisor of the work, Prof. Martti Toivakka. The past 12 years have gone quickly and I have enjoyed our collaboration with various trips to conferences, organizing conferences and intensive courses in Turku, supervising joint students, and learning a lot. I would also like to thank Prof. Jouko Peltonen for the collaboration especially in 2008–2011 with wettability and printability studies.

PhD Mari Nurmi has been the cornerstone for the practicalities at the lab and Björn ÄV Friberg has assisted in technical aspects, and not forgetting the performances in the departmental parties! Jani Kniivilä has been a marvel with computers & coding. PhD Roger Bollström was a co-author and colleague for several years. I would like to thank all co-authors, and especially those, whose work I had the privilege to supervise: PhD Milena Stepien, PhD Katariina Torvinen, PhD Dimitar Valtakari, and PhD Kofi J. Brobbey.

I would like to thank Prof. Jyrki M. Mäkelä from Tampere University for a long-time collaboration with liquid flame spray (LFS) deposition of nanoparticles on various substrates with applications ranging from controlled wetting and Raman scattering to antimicrobial activity. I would also like to acknowledge other collaborators from Tampere University: Prof. Jurkka Kuusipalo, PhD Mikko Tuominen, PhD Hannu Teisala, PhD Mikko Aromaa, PhD Turkka Salminen, and MSc Janne Haapanen.

I would like to express my deep gratitude to Prof. Jun Uozumi from the Hokkai-Gakuen University in Sapporo. I have had two wonderful opportunities to visit Japan for a longer time in 2011–2012 and in spring 2016. I have enjoyed your warm hospitality and guidance to both science and Japanese way of living with various discussions from Japanese trains (shinkansens), history, and culture. Dōmo arigatō.

Collaboration with Prof. Takeya Unuma from the Nagaoka University of Technology is greatly appreciated, being established during the Japan-Finland Optics in Engineering (OIE) symposia. I would also like to thank all Finnish and Japanese colleagues who have been active in the OIE symposium series - especially the role of Prof. Emeritus Kai-Erik Peiponen has been paramount. I feel that there is a mutual connection between the Japanese and Finns with many similarities in culture, and I look forward to meeting you again in future OIE meetings.

Financial support from various sources is greatly acknowledged. This work has been supported by the Finnish Cultural Foundation, Academy of Finland, Japan Society for Promotion of Science, The Scandinavia-Japan Sasakawa Foundation, Åbo Akademi, and Åbo Akademi Foundation.

Finally, the role of family can never be underestimated. I have been blessed with having a loving and patient wife Ulriikka (which, honestly, is not always easy with me), and I would like to thank you for all the support during these years. We are fortunate to have two adorable, beautiful, smart, fun, and magnificent kids, Vilppu and Viola, whose proud father I have the honor to be. Little did I know about the meaning of love before meeting you two.

ABSTRACT

This work concentrated on three nanophotonic applications based on printed and coated functionality on natural fibre based substrates. Hence, the thesis deals with three emerging fields: nanotechnology, nanophotonics, and sustainable materials. Nanotechnology tools have been developed over the past few decades increasing tremendously our abilities to control matter in nanoscale. This has resulted in the growth of nanophotonics, i.e. how light can be controlled by nanoscale structures and particles. This work concentrates on TiO_2 and silver nanoparticles, and their applications on paperboard substrate. Demands for sustainability have grown significantly in recent years with growing population and emerging environmental issues. Nanotechnology is an ideal tool for promoting sustainability: with less material and energy consumption one can generate the same or even enhanced properties. Combining such nanoscale structures with renewable materials provides a double advantage compared to the traditional solutions.

First, photocatalytic activity of liquid flame spray (LFS) deposited TiO_2 nanoparticles on paperboard was utilized for controlled wettability. It has been shown earlier that it is possible to convert an initially superhydrophobic surface into a highly hydrophilic one by ultraviolet A (UVA) irradiation. However, this process is reversible and the initial superhydrophobicity is returned within 60 days in storage. In this work a protocol was developed for making the wettability conversion permanent by first stage wetting, i.e. by exposing the UVA irradiated TiO_2 nanoparticles to water that removed the nanoparticles from the irradiated area permanently. Additionally, durability of such nanoparticle coated paperboard under compression was studied.

Surface-enhanced Raman scattering (SERS) activity was demonstrated by LFS deposited silver nanoparticles on glass substrate, thereafter expanded to paperboard surfaces. A problem with paperboard for SERS analysis is background luminescence, which is typically orders of magnitude larger than the Raman signal, and which thereby easily dominates the measured spectrum. Two different solutions for SERS active paperboard substrates were developed. First, inkjet printing with commercial silver nanoparticle ink was found suitable for SERS activity but only with a full silver coverage on paperboard blocking the luminescence from the base paperboard. A more cost-effective solution was developed by using a simple carbon coating by flexography that allowed even individual LFS deposited silver nanoparticles for SERS measurements on paperboard with significantly reduced silver amount and consequently, cost.

Finally, commercial TiO_2 nanoparticles were used together with methylene blue (MB) organic dye. MB has a distinct blue color in the oxidized form that can be converted to the transparent leucomethylene blue form by UVA activation together with TiO_2 nanoparticles. Therefore, functional ink combining MB with TiO_2 nanoparticles was shown to be suitable for cost-efficient oxygen indicators. Both reverse gravure coated and flexographic printed indicator labels were demonstrated that are suitable for simple oxygen indicators, for example, in modified atmosphere packages.

The use of metal and metal oxide nanostructures as functional light-activated materials enables creation of both cost-efficient and environmentally sound products, which can be widely used in society enabling a break-through in transformation from the current fossil fuel based economy to a solar driven economy. Therefore, as a summary, it is believed that the results of the thesis can lay ground for the development of new large-scale, nanostructured light-activated materials on natural fibre based substrates providing sustainable solutions for future generations.

SVENSK SAMMANFATNING

Detta arbete koncentrerade sig på tre nanofotoniska applikationer som baserar sig på tryckt och bestruken funktionalitet på naturfiberbaserade substrat. Avhandlingen behandlar tre nya områden: nanoteknologi, nanofotonik och hållbara material. Nanotekniska verktyg har utvecklats under de senaste decennierna och ökat enormt vår förmåga att kontrollera materia i nanoskala. Detta har resulterat i tillväxt av nanofotonik, dvs. hur ljus kan styras av strukturer och partiklar i nanoskala. Detta arbete koncentrerar sig på TiO_2- och silvernanopartiklar och deras applikationer på kartongunderlag. Kraven på hållbarhet har vuxit betydligt under de senaste åren samtidigt med ökande befolkning och växande miljöproblem. Nanoteknologi är ett idealt verktyg för främjande av hållbarhet: med mindre material- och energiförbrukning kan man generera samma eller till och med förbättrade egenskaper. Genom att kombinera sådana strukturer i nanoskala med förnybara material fördubblas fördelen jämfört med de traditionella lösningarna.

Fotokatalytisk aktivitet av TiO_2-nanopartiklar som utfällts med flytande flamspray (LFS) på kartong användes för kontrollerad vätningsförmåga. Det har tidigare visats att det är möjligt att konvertera en initialt superhydrofob yta till i en hög grad hydrofil yta via ultraviolett A (UVA)-aktivering. Denna process är dock reversibel och den initiala superhydrofobiciteten återkommer inom 60 dagars lagring. I detta arbete utvecklades en metod för att göra vätningsförmågans konvertering permanent genom vätning av första steget, dvs. genom att utsätta de UVA-aktiverade TiO_2-nanopartiklarna för vatten som permanent avlägsnade nanopartiklarna från det strålade ytan. Dessutom undersöktes hållbarheten för en nanopartikelbelagd kartong under kompression. Aktiviteten av ytförstärkt Raman-spridning (SERS) demonstrerades med hjälp av LFS-deposition av silverpartiklar på glassubstrat och senare på kartongytor. Ett problem med kartong för SERS-analys är bakgrundsluminescensen som är normalt några storleksordningar större än Raman-signalen och därför enkelt dominerar det mätta spektrumet. Två olika lösningar för SERS-aktiva kartong utvecklades. Den första var bläckstråletryckning med en kommersiell nanopartikulär silvertryckfärg som var lämplig för SERS-aktivitet men endast då kartongytan var totalt täckt så att luminescensen från kartongen blockerades. En mer kostnadseffektiv lösning utvecklades genom att använda en enkel kolbeläggning med hjälp av flexografi som möjliggjorde även SERS-analys av individuella LFS-deponerade silverpartiklar på kartong vilket reducerade silvermängden och kostnaderna. Slutligen användes kommersiella TiO_2-nanopartiklar tillsammans med ett organiskt färgämne, metylenblå (MB). MB har en distinkt blå färg i oxiderad form som kan omvandlas till den genomskinliga leukometylenblå genom UVA-aktivering tillsammans med TiO2-nanopartiklar. Därför visade sig det funktionella bläcket som kombinerar MB med TiO_2-nanopartiklar vara lämpligt för kostnadseffektiva syreindikatorer. Både omvänd gravyrbelagda och flexografitryckta indikatoretiketter, som är lämpliga för t.ex. enkla syreindikatorer i förpackningar med modifierad atmosfär, demonstrerades.

Användning av metall- och metalloxidnanostrukturer som funktionella ljusaktiverade material möjliggör skapande av både kostnadseffektiva och miljöanpassade produkter som kan i stor utsträckning användas i samhället, och som möjliggör ett genombrott i omvandlingen från en ekonomi baserad på fossilt bränsle till en solstyrd ekonomi. Sammanfattningsvis, resultaten från denna avhandling kan antas ge en bas för utveckling av nya storskaliga, nanostrukturerade ljusaktiverade material på naturfiberbaserade substrat som ger hållbara lösningar för kommande generationer.

LIST OF PUBLICATIONS

Publication I

M. Stepien, J. J. Saarinen, H. Teisala, M. Tuominen, M. Aromaa, J. Haapanen, J. Kuusipalo, J. M. Mäkelä, and M. Toivakka, "Compressibility of porous TiO_2 nanoparticle coating on paperboard," *Nanoscale Research Letters* **8**, 444 (2013).

Publication II

J. J. Saarinen, D. Valtakari, J. Haapanen, T. Salminen, J. M. Mäkelä, and J. Uozumi, "Surface-enhanced Raman scattering active substrates by liquid flame spray deposited and inkjet printed silver nanoparticles," *Optical Review* **21**, 339–344 (2014).

Publication III

D. Valtakari, M. Stepien, J. Haapanen, H. Teisala, M. Tuominen, J. Kuusipalo, J. M. Mäkelä, M. Toivakka, and J. J. Saarinen, "Planar fluidic channels on TiO_2 nanoparticle coated paperboard," *Nordic Pulp and Paper Research Journal* **31**, 232–238 (2016).

Publication IV

J. J. Saarinen, D. Valtakari, S. Sandén, J. Haapanen, T. Salminen, J. M. Mäkelä, and J. Uozumi, "Roll-to-roll manufacturing of disposable surface-enhanced Raman scattering (SERS) sensors on paper based substrates," *Nordic Pulp and Paper Research Journal* **32**, 222–228 (2017).

Publication V

J. J. Saarinen, T. Remonen, D. Tobjörk, H. Aarnio, R. Bollström, R. Österbacka, and M. Toivakka, "Large-scale roll-to-roll patterned oxygen indicators for modified atmosphere packages", *Packaging Technology and Science* **30**, 219–227 (2017).

AUTHOR'S CONTRIBUTION

Publication I

The author was responsible for planning the experiments together with the co-authors. The LFS nanoparticle deposition was carried out at the Tampere University of Technology. The author carried out data interpretation of the experimental results. The manuscript was mainly written by the author.

Publication II

The author planned the experiments and coordinated the sample manufacturing and experiments. The LFS nanoparticle deposition and the SERS measurements were carried out at the Tampere University of Technology. The author was responsible for data analysis and interpretation. The author wrote the manuscript.

Publication III

The author planned the experiments and coordinated the sample manufacturing and experiments. The LFS nanoparticle deposition was carried out at the Tampere University of Technology. The author analyzed the data and wrote the first draft of the manuscript.

Publication IV

The author planned the experiments and coordinated the sample manufacturing and experiments. The LFS nanoparticle deposition and the SERS measurements were carried out at the Tampere University of Technology. The author was responsible for data analysis and interpretation. The author wrote the manuscript.

Publication V

The author took part in data analysis with the co-authors. The data interpretation was carried out by the author, and the manuscript was mainly written by the author.

SUPPORTING JOURNAL PUBLICATIONS

S1. J. Haapanen, M. Aromaa, H. Teisala, P. Juuti, M. Tuominen, M. Sillanpää, M. Stepien, J. J. Saarinen, M. Toivakka, J. Kuusipalo, and J. M. Mäkelä, "On the limit of superhydrophobicity: defining the minimum amount of TiO_2 nanoparticle coating," *Materials Research Express* **6**, 035004 (2019).

S2. K. J. Brobbey, J. Haapanen, M. Gunell, J. M. Mäkelä, E. Eerola, M. Toivakka, and J. J. Saarinen, "One-step flame synthesis of silver nanoparticles for roll-to-roll production of antibacterial paper," *Applied Surface Science* **420**, 558–565 (2017).

S3. J. Haapanen, M. Aromaa, H. Teisala, M. Tuominen, M. Stepien, J. J. Saarinen, M. Heikkilä, M. Toivakka, J. Kuusipalo, and J. M. Mäkelä, "Binary TiO_2/SiO_2 nanoparticle coating for controlling the wetting properties of paperboard," *Materials Chemistry and Physics* **149–150**, 230–237 (2015).

S4. M. Stepien, G. Chinga-Carrasco, J. J. Saarinen, H. Teisala, M. Tuominen, M. Aromaa, J. Haapanen, J. Kuusipalo, J. M. Mäkelä, and M. Toivakka, "Wear resistance of wettability-controlling nanoparticle coatings on paperboard," *Wear* **307**, 112–118 (2013).

S5. D. Valtakari, R. Bollström, M. Tuominen, H. Teisala, M. Aromaa, M. Toivakka, J. Kuusipalo, J. M. Mäkelä, J. Uozumi, and J. J. Saarinen, "Flexographic printing of PEDOT:PSS on coated papers for printed functionality," *Journal of Print Media and Technology Research* **2**, 7–13 (2013).

S6. M. Stepien, J. J. Saarinen, H. Teisala, M. Tuominen, M. Aromaa, J. Haapanen, J. Kuusipalo, J. M. Mäkelä, and M. Toivakka, "ToF-SIMS analysis of UV-switchable TiO_2-nanoparticle coated paper surface," *Langmuir* **29**, 3780–3790 (2013).

S7. M. Stepien, J. J. Saarinen, H. Teisala, M. Tuominen, M. Aromaa, J. Kuusipalo, J. M. Mäkelä, and M. Toivakka, "Surface chemical analysis of photocatalytic wettability conversion of TiO_2 nanoparticle coating," *Surface & Coatings Technology* **208**, 73–79 (2012).

S8. M. Stepien, J. J. Saarinen, H. Teisala, M. Tuominen, M. Aromaa, J. Kuusipalo, J. M. Mäkelä, and M. Toivakka, "Surface chemical characterization of nanoparticle coated paperboard," *Applied Surface Science* **258**, 3119–3125 (2012).

S9. J. J. Saarinen, P. Ihalainen, A. Määttänen, R. Bollström, and J. Peltonen, "Printed sensor and electric field assisted wetting on a natural fibre based substrate," *Nordic Pulp and Paper Research Journal* **26**, 133–141 (2011).

S10. M. Stepien, J. J. Saarinen, H. Teisala, M. Tuominen, M. Aromaa, J. Kuusipalo, J. M. Mäkelä, and M. Toivakka, "Adjustable wettability of paperboard by liquid flame spray nanoparticle deposition," *Applied Surface Science* **257**, 1911–1917 (2011).

SUPPORTING CONFERENCE PUBLICATIONS

C1. J. J. Saarinen, B. K. Brobbey, J. Haapanen, M. Gunell, E. Eerola, P. Huovinen, and J. M. Mäkelä, "Liquid flame spray (LFS) deposited nanoparticles on natural fibre based substrates for antimicrobial activity," in *ACS 2018 National Meeting and Exposition* (ACS, New Orleans, LA, United States, March 18–22, 2018).

C2. J. J. Saarinen, D. Valtakari, R. Bollström, M. Stepien, J. Haapanen, J. M. Mäkelä, and M. Toivakka, "Roll-to-roll application of photocatalytic TiO_2 nanoparticles for printed functionality," in *Technical Proceedings of the TechConnect World Innovation Conference & Expo – Nanotech 2016, eISBN: 9780997511734* (TechConnect, Washington D.C., United States, May 22–25, 2016), Vol. 4, CRC Press, pp. 47–50.

C3. J. J. Saarinen, D. Valtakari, M. Stepien, M. Tuominen, H. Teisala, J. Haapanen, J. Kuusipalo, J. M. Mäkelä, and M. Toivakka, "Planar fluidic channels on TiO_2 nanoparticle coated paperboard," in *IPCCS2015 9th International Paper and Coating Chemistry Symposium* (IPCCS / IPPC, Tokyo, Japan, October 29–31, 2015), p. 13.

C4. J. J. Saarinen, T. Remonen, D. Tobjörk, R. Bollström, R. Österbacka, and M. Toivakka, "A novel process for UV light activated oxygen indicators for modified atmosphere packages", in *TAPPI Paper Conference and Trade Show, PaperCon 2015, ISBN: 9781510818873* (TAPPI, Atlanta, GA, United States, April 19-22, 2015), Vol. 1, TAPPI Press, pp. 21–32.

C5. J. J. Saarinen, D. Valtakari, S. Sánden, J. Haapanen, T. Salminen, and J. M. Mäkelä, "Roll-to-roll manufacturing of silver nanoparticle based SERS sensors on paper substrates", in *Label-Free Technologies* (Elsevier, Cambridge, MA, United States, March 12–14, 2015).

C6. J. J. Saarinen, D. Valtakari, J. Haapanen, T. Salminen, J. M. Mäkelä, and J. Uozumi, "SERS active substrates by liquid flame spray and inkjet printed silver nanoparticles," in *OSA Advanced Photonics Congress: Optical Sensors 2013 Technical Digest*, (Optical Society of America, Puerto Rico, PR, United States, July 14–19, 2013), SW1B.4.

LIST OF ABBREVIATIONS

AFM	atomic force microscopy
$AgNO_3$	silver nitrate
AgNP	silver nanoparticle
ALD	atomic layer deposition
BE	binding energy
BSE	back-scattered electron
CO_2	carbon dioxide
CV	crystal violet
CVD	chemical vapor deposition
DDA	discrete dipole approximation
DPL	dip-pen lithography
DS	drop spacing
DSSC	dye-sensitized solar cell
E. coli	*Escherichia coli*
EDTA	ethylenediaminetetraacetic acid
EG	ethylene glycol
ELISA	enzyme-linked immunosorbent assay
ESB	energy and angle selective backscattered electron
FESEM	field emission scanning electron microscopy
FSP	flame spray pyrolysis
ICP	inductively coupled plasma
IoT	internet of things
IPA	isopropanol
IPCC	Intergovernmental Panel on Climate Change
KE	kinetic energy
LFS	liquid flame spray
LMB	*leuco* form (methylene blue)
LSPR	localized surface plasmon resonance
LWC	light-weight coated
MAP	modified atmosphere package
MB	methylene blue
MBE	molecular beam epitaxy
O/C	oxygen to carbon ratio
OBA	optical brightening agent
PCA	principal component analysis
PDMS	polydimethylsiloxane
PET	poly(ethylene terephthalate)
PMMA	polymethylmethacrylate
POC	point-of-care
PVD	physical vapor deposition
RFID	radio-frequency identification
RG	reverse gravure
RhB	Rhodamine B

SA	styrene-acrylic
SB	styrene-butadiene
SE	secondary electron
SEM	scanning electron microscopy
SiO_2	silica
SLIPS	slippery liquid infused porous surfaces
SP	spray pyrolysis
SERS	surface-enhanced Raman scattering
STM	scanning tunneling microscopy
TERS	tip-enhanced Raman spectroscopy
TiO_2	titanium dioxide
ToF-SIMS	time-of-flight secondary ion mass spectroscopy
TTIP	titanium(tetra)isopropoxide
UHV	ultrahigh vacuum
UVA	ultraviolet A
WCA	water contact angle
XPS	X-ray photoelectron spectroscopy

Contents

Chapter 1

Introduction

Nanophotonics is an emerging field that has a wide range of applications from solar energy conversion and optical sensing to optical telecommunications and computing. Many of our everyday life objects depend on nanotechnology and nanophotonics: for example, modern cell phones are powered by integrated circuits containing billions of transistors packed on roughly one square centimeter area, and internet connections heavily rely on optical fibres. Many summer cottages in Finland make their electricity using solar cells based on nanophotonic integration.

Within the past few decades our abilities to manufacture nanoscale structures has expanded tremendously. In his famous keynote talk at the Caltech in December 1959, late Nobel laureate Richard Feynman considered possibilities for nanoscale engineering [1]. His thought experiment summarized it well: "*The principles of physics, as far as I can see, do not speak against the possibility of maneuvering things atom by atom. It is not an attempt to violate any laws; it is something, in principle, that can be done; but, in practice, it has not been done because we are too big.*" In the following six decades since Feynman's talk, both nanoscale measurement and manufacturing tools have been developed, and nowadays abilities to modify matter down to an individual atom level are available.

Nature has mastered nanoscale engineering for billions of years. We all are based on extremely well designed nanoscale structures that are made using a bottom-up route in aqueous solution i.e. nature starts with individual molecules that are assembled into larger functional units, organs, and organisms guided by the genetic information encoded into the DNA. This is contrary to the typical man-made nanoscale structures that use a top-down approach in which one starts with large macroscopic particles and then by removing material at desired locations one ends up with nanoscale features. For example, the integrated chips in our cell phones use such an approach in which a large silicon substrate is covered with multiple thin films before exposure to lithographic processes for making the sources, drains, and gates for the billions of field-effect transistors in today's mobile phone processors.

In particular, natural processes are sustainable: all natural processes are widely distributed and function in a zero-waste protocol in which the waste from one or more organisms is the source material for another. On the contrary, man-made processes are typically heavily concentrated in industrial plants resulting in a large amount of waste. This has been realized within the past few decades as mankind is running out both renewable and especially non-renewable raw materials.

In recent years circular economy, mimicking the natural approach, has generated large interest to improve sustainability with increasing population and demand, and in Finland the world's first roadmap for circular economy was released in 2016 [2] .

One consequence of following unsustainable action is global warming. The Intergovernmental Panel on Climate Change (IPCC) released a report in 2018 [3] indicating the changes required to limit the temperature increase to 1.5°C. The IPCC also reported earlier [4] that 65% of the carbon dioxide (CO_2) emissions result from fossil fuels and industrial processes. During the past hundred years the annual global carbon emissions have increased 10-fold up to 10 billion metric tonnes [5], and the CO_2 level in the atmosphere has increased from pre-industrial 280 ppm to more than 400 ppm due to wide use of fossil fuels such as coal, oil, and natural gas. There has been several studies indicating the outcomes of uncontrolled temperature increase: the first signs are the deadly heatwaves throughout the world [6,7], especially in Australia in the Antipodean summer of 2019, early 2020, with bush fires on a land area comparable to Finland.

This highlights the urgent need for a sustainable transformation from fossil fuel based economy to carbon neutral solutions. Solar economy offers a tremendous opportunity for achieving this goal. The average solar energy intensity reaching the Earth is approximately 1 360 W/m^2 [8]. To harvest this energy, solar cells have been intensely investigated since the 1950s, and the best available solar power conversion efficiencies of multi-junction crystalline cells is approaching 50% [9]. To reduce the cost of solar cells, a dye-sensitized solar cell (DSSC) structure based on a colloidal titanium dioxide (TiO_2) solution was proposed by O'Regan and Grätzel in 1991 [10]. There has been extensive research on DSSC cells [11] within the past 25 years but, unfortunately, the limitations in the available photosensitizer dyes have kept the power conversion efficiency around 10%.

Alternatively, solar energy can be used to drive heterogeneous catalytic chemical reactions on surfaces via photocatalytic activation. Photocatalysis on TiO_2 surfaces is a well-known phenomenon since the seminal work in the early 1970s [12, 13]. TiO_2 is nowadays a widely used material due to its nontoxicity, chemical and biological inertness, sufficient photostability, and strong oxidizing potential to catalyze various redox reactions while at the same time having a sufficiently large bandgap (3.2 eV for anatase crystalline form corresponding to 387 nm in the ultraviolet A (UVA) range) [14]. This is a significant bottleneck since only 3—5% of sunlight is in the UV range [15] for excitation of the electron-hole pairs in TiO_2 responsible for reduction and oxidation reactions on the surface, respectively.

To overcome the large bandgap in TiO_2, several approaches have recently been taken including doping, surface modification, formation of black TiO_2, ion implantation, or composite semiconductors [16, 17]. Unfortunately, the benefits of the lower bandgap are often diminished by a higher recombination rates of the generated electron-hole pairs limiting the achievable overall efficiency.

Metal nanoparticles, which exhibit localized surface plasmon resonance (LSPR), are effective in concentrating electromagnetic radiation, i.e. inducing strong local electric fields in small volumes. LSPR in metallic nanoparticles has been utilized for decades, e.g. in surface-enhanced Raman scattering (SERS) [18]. More recently, plasmonic nanoparticles have found applications for enhanced photocatalytic activity as they can be a source of hot carriers (electrons and holes) that can transfer from the plasmonic nanostructure into the neighboring metal oxide. Designs for extracting both hot electrons [19, 20] and hot holes [21] for photocatalytic activity at visible wavelengths have been under intense research during the past few years. Such indirect photo-

catalysis can take advantage of both metallic and semiconducting structures, and recently also bimetallic (Ag/Pt) particles were investigated combining plasmonic and catalytic functions into a single nanostructure [22]. It has also been shown that a direct photocatalysis can take place on top of plasmonic nanostructures [23,24]. To fully exploit the possibilities of metal and metal oxide nanomaterials, a more detailed understanding of key physico-chemical properties is required. Understanding the structure-property connection requires information about the driving forces of the nanophotonic response.

Sustainability can be improved by combining solar energy driven systems into substrates based on renewable raw materials and energy sources. Forests have traditionally been a source for well-being in Finland, and cellulose is the most abundant biopolymer on Earth. Annually more than 100 million cubic meters of fresh wood biomass is grown in Finland alone from which approximately 80% is harvested. A large transformation of the forest-products industry sector has taken place within the past two decades as the growth of electronic media has resulted in a rapid decline in demand of traditional printing paper grades. This has resulted in closures of several paper mills but also generated new product portfolios ranging from micro- and nanofibrillated cellulose and cross-laminated timber products to wood-based chemicals and biofuels.

This thesis deals with nanophotonic applications on paperboard concentrating on TiO_2 and silver nanoparticles. Three different applications will be considered: first, photocatalytically controlled wettability of TiO_2 nanoparticle coated paperboard followed by SERS active substrates by silver nanoparticles. Finally, TiO_2 nanoparticles together with methylene blue organic dye can be used as a simple oxygen indicator, for example, in modified atmosphere packages. Combining nanophotonic applications in renewable and recyclable substrates can provide significant added value and show avenues towards a both economically and ecologically sustainable future.

The aims of this study are as follows:

1. Develop light-activated metal and metal oxide nanoparticle coatings on paperboard
2. Identify the key structure-property mechanisms that control the photonic response in such nanostructured media
3. Demonstrate controlled wetting and Raman sensing on such nanoparticle functionalized paperboard

Chapter 2

Review of Literature

2.1 Basics of nanotechnology

Nanotechnology has gained widespread interest within the past few decades due to the new properties that can be achieved via nanoscale engineering and structures. There are two main pathways why matter behaves differently in nanoscale compared to macroscale. First, the ratio of surface to bulk atoms grows as the dimensions of structures are minituarized. For example, MgO and CaO nanocrystals were studied in different sizes and the ratio of surface atoms was decreased from more than 90% to less than 10% as the particle diameter was increased from 1 nm to 15 nm [25]. Secondly, quantum phenomena, which are typically observed only in atomic scale, can manifest themselves through into resulting macroscale properties.

Gold is a well-known soft metal with distinct yellowish color. However, the melting point of gold was significantly reduced from the bulk value of 1 064°C to less than 500°C as the diameter of gold nanoparticles was reduced to less than 5 nm [26]. Additionally the color of gold surface can be altered by nanoscale structures: engraving nanodiscs with various diameters around 100 nm can be used for plasmonic control of the reflected color and various colored surfaces can be generated [27]. In a similar fashion the diameter of silver nanoparticles can be used to control Rayleigh scattering that resulted in different colors [28]. These colors in metallic nanostructures are caused by the disturbances induced into the electron mean free path by the physical boundaries, i.e. the electron oscillations caused by the coupled electromagnetic radiation is affected by collisions with the grain boundaries. In silver and gold the electron mean free paths in bulk metals were calculated to be 53.3 nm and 37.7 nm, respectively [29].

2.1.1 Top-down vs. bottom-up manufacturing routes

Nanoscale structures can be achieved by two different manufacturing routes. The top-down approach starts with a macroscopic unit that is reduced down to nanoscale. There are several ways to achieve this, such as applying mechanical, high energy, chemical, and lithographical processes. Electron beam lithography is widely used in manufacturing integrated circuits [30] whereas mechanical treatment with enzymes is typically used for making cellulose nanofibrils [31]. The bottom-up route, by contrast, starts with individual atoms or molecules that are assembled into a larger functional unit. Man-made structures by this route can be achieved

by dip-pen lithography (DPL), chemical / physical vapor deposition (CVD/PVD), atomic layer deposition (ALD), molecular beam epitaxy (MBE), or self-assembly.

Nature has mastered bottom-up manufacturing in aqueous solution for billions of years, and mimicking natural structures, i.e. biomimetics has been a focus of intense interest in recent years [32]. Hierarchical structures combining both micro- and nanoscale structures are typically found in nature that result in extraordinary properties such as the extreme water repellency of the lotus leaf [33], structural color in morpho butterflies and pollia fruit [34], brilliant whiteness in beetles [35], and even in camouflage [36].

Nanoparticles can be synthesized in various ways, ranging from wet chemical sol-gel synthesis and laser ablation to epitaxy and powder technologies.

2.1.2 Liquid flame spray (LFS) deposition of nanoparticles

Spray pyrolysis (SP) techniques have been developed intensively since the 1980s. In SP, a heated laminar flow carries the precursor aerosol into the furnace. Aerosol, which can be formed, e.g. using ultrasonic, pneumatic or electrostatic assistance, is rapidly heated forming solid nanoparticles [37, 38]. SP offers high versatility with easily controllable particle size distribution and composition range of various metal and metal oxide nanoparticles. Typically the furnaces operate within a temperature range of 100–500°C [39] allowing nanoparticle deposition on relatively heat-sensitive materials. The SP technique allows also deposition of tailorable and multicompound structures including core-shell, nanowires, and thin film deposition; for details, see a recent review [40].

Flame spray pyrolysis (FSP) differs from the conventional SP, in that, instead of an oven, the heat is generated by the flame followed by the thermomechanical reactions leading to nanoparticle deposition. Seminal work using a flame was carried out by Ulrich in 1971 [41] for preparing silica (SiO_2) particles from silicon tetrachloride ($SiCl_4$). Flame based methods for deposition of nanoparticles provide a cost-effective, large-scale means for production of nanomaterials up

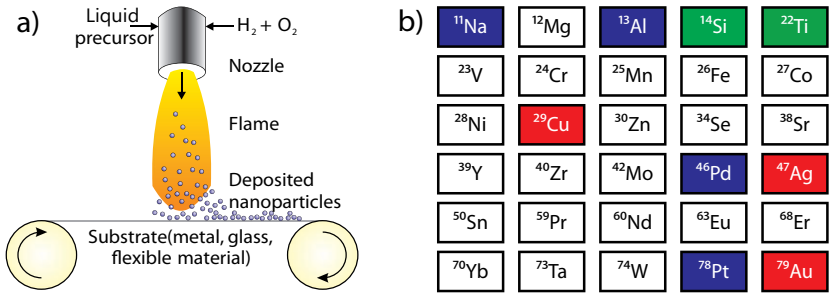

Figure 2.1: a) Schematic of LFS nanoparticle deposition in a roll-to-roll process flow, with a matrix of suitable elements for nanoparticle deposition by the LFS process b). The most typical Raman active metals are displayed by red whereas more recently explored metals for Raman activity are displayed by blue. The oxides used for controlled wettability are displayed by green.

to millions of tonnes annually [42, 43]. In FSP, a metal salt precursor is sprayed as a fine mist into a high temperature flame for nanoparticle formation. Thermophoretic deposition of porous functional films was demonstrated as a one-step fabrication of Au/TiO_2 microreactors [44].

Liquid flame spray (LFS) deposition of nanoparticles has been developed at the Tampere University of Technology, Finland since the 1990s. LFS is a subgroup of FSP techniques with the main difference compared to conventional FSP being in the aerosol generation: in LFS, one of the combustion gases is also the atomizing gas of pneumatically sprayed precursor solution, whereas in FSP an additional atomizer is typically used. Figure 2.1a) shows a schematic figure of the LFS deposition system. A precursor is fed into the high temperature and high velocity flame in which evaporation and nucleation takes place. Thermal decomposition of precursor solution is followed by formation of solid nanoparticles given by the following overall reactions of titanium(tetra)isopropoxide (TTIP) precursor and silver nitrate ($AgNO_3$) for TiO_2 and silver nanoparticles, respectively:

$$Ti(OC_3H_7)_4 \rightarrow TiO_2 + 4C_3H_6 + 2H_2O \tag{2.1}$$

$$AgNO_3 \rightarrow Ag + NO_2 + O_2 \tag{2.2}$$

$$AgNO_3 + H_2 \rightarrow Ag + NO_2 + H_2O \tag{2.3}$$

Compared to the hydrolysis of $TiCl_4$ based precursors, TTIP has an advantage of significantly lower thermal decomposition temperature down to 100°C [45]. For silver, pure, densely packed and non-agglomerated particles were produced at and above 900°C when using air as carrier gas with sufficiently low residence times in the furnace [46]. However, presence of hydrogen reduced the equilibrium of thermal decomposition of silver nitrate from 400°C to room temperature [47]. The morphology of the LFS deposited TiO_2 and silver nanoparticles is shown by the scanning electron microscope (SEM) image in Fig. 2.2. A clear difference in the particle morphology can be seen as TiO_2 nanoparticles form a highly porous network, whereas silver nanoparticles deposit as individual or aggregated (fused) nanoparticles.

The highest temperatures in the flame reach close to 3 000 K approximately 5 cm distance from the burner [48]. However, flame temperature decays quickly to 1 000 K as distance is increased to 20 cm. Hence, even heat-sensitive materials such as paper or plastic film can be function-

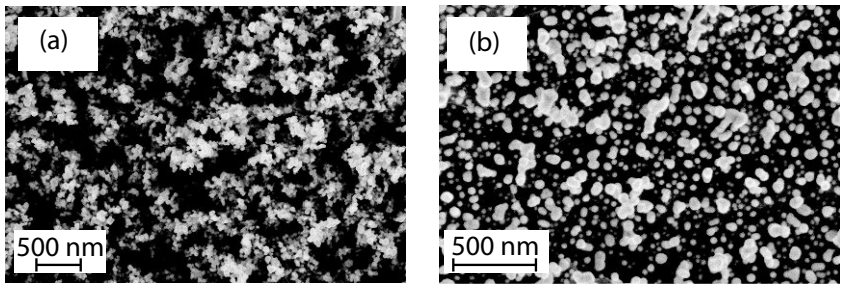

Figure 2.2: SEM images of LFS deposited a) highly porous TiO_2 nanoparticle network and b) individual and aggregated silver nanoparticles.

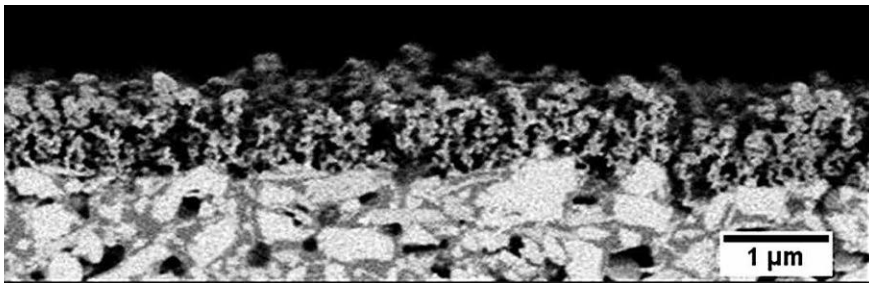

Figure 2.3: Cross-sectional image of LFS deposited TiO_2 layer on top of pigment coated paperboard (image courtesy of PhD Milena Stepien [57]).

alized with LFS deposited nanoparticles as long as the distance from the burner and exposure time to the flame, in turn, are kept sufficiently long and short, respectively. In addition, high purity samples can be achieved with no organic residues [49] by the flame based methods. A recent X-ray photoelectron spectroscopy (XPS) study of LFS deposited silver nanoparticles [50] showed that more than 90% of the deposited particles were metallic silver with approximately 7% in AgO_2 state and less than 1% in AgO state.

The benefits of the LFS process include rapid deposition, scalability, versatility, and possibility for generating multicompound structures [51–53]. The versatility of the LFS method is displayed in Fig. 2.1 b) with a matrix of suitable metal and metal oxide particles for Raman activity and controlled wettability, respectively. The particle size can easily be controlled from 2 to 200 nm by process parameters such as precursor concentration and feeding rate, burner distance to the deposition substrate, and gas flow rates. The size distribution of particles can be single- or multiple peaked depending on the burner temperature and vapour pressures of the source materials [54]. For example, a single-peaked distribution of silver nanoparticles by LFS has been demonstrated [55]. From the LFS generated nanoparticles, a typical yield onto the surface is commonly in the range of 5–20% [56]. The LFS deposition of nanoparticles can be carried out either in a batch-type process using a rotating carousel or in a continuous roll-to-roll application. In both cases the deposited nanoparticle amount can easily be controlled by the track/substrate speed and the number of passes through the flame.

A cross-sectional SEM image of highly porous LFS deposited TiO_2 nanoparticles is displayed in Fig. 2.3. It is noteworthy that the SEM image here is taken without sputtering by carbon or gold. The LFS deposited TiO_2 layers had a thickness of approximately 600 nm [Paper I]. This information can be combined with inductively coupled plasma (ICP) analysis indicating 100 mg/m^2 coating amount: assuming anatase crystalline form with density of 3.89 g/cm^3 resulted in the average porosity of 96%. This is in good agreement with previous experiments of the FSP deposited Pt/SnO_2 gas sensors having a high porosity up to 98% [58]. High porosity was also observed in simulation of nanoparticle deposition with Brownian motion dynamics that showed a packing density (= 1 - porosity) between 2–15% [59].

The adhesion of nanoparticles onto the solid substrate is mainly due to van der Waals forces that are weak compared to chemical bonds. Therefore, several strategies have been utilized to improve LFS nanoparticle adhesion ranging from partial heat-induced embedding into a soft

polymer matrix during the deposition [60] to ALD [50] and plasma [61] coatings. High temperature deposition of TiO_2 nanoparticles at 400°C reduced the porosity from 98% to 95% compared to 100°C deposition [62] while a partial sintering of the particles improved the mechanical stability of the deposited layer for DSSC application. Alternatively, a secondary flame can be used to anneal the deposited nanoparticle layer [63]. A secondary flame was also used in combination with a shadowing mask for generating micropatterned nanoparticle depositions on Si-wafer [64].

LFS deposited nanoparticles have found various applications in recent years ranging from glass coloring [65] and erbium-doped fiber amplifiers [54] to functional coatings with controlled wettability from superhydrophobic to highly hydrophilic surfaces on paperboard [66,67], controlled printability [68], and antibacterial applications [55]. For a summary of LFS applications, see a recent review [69].

2.2 Light: Optics and photonics

2.2.1 Light fundamentals

Light is a form of electromagnetic radiation whose behavior is governed by the four Maxwell equations: two divergence equations complemented with two curl equations coupling the vectorial electric and magnetic fields. Unfortunately, these four equations, albeit simple in their analytic form, are difficult to solve, and only few closed form solutions are available in specific circumstances. Therefore, heavy numerical investigations are often required for detailed optics and photonics modeling taking into account the sufficient boundary conditions, i.e. along the interface continuity of the tangential component of the electric field and magnetic field for a dielectric interface.

The optical interfaces are defined by the difference in the refractive index. As a photon hits such an interface, it can transmit through the interface, be reflected back to the incoming medium, or be absorbed into the medium. Light behavior in complex media, such as nanostructured or turbid media, results from multiple reflections at different interfaces. This is called *scattering* that can be either elastic or inelastic in nature. Elastic scattering covers Rayleigh scattering from molecules that explains, for example, why sky is blue or snow is white. Rayleigh scattering is inversely proportional to the fourth power of the wavelength, and thus far away from the sun, the blue components (short wavelength) experience a higher scattering probability and result in the blue color of the sky. Another example of the importance of air voids is snow: being highly porous there is a large number of scattering centers available and for a white light the appearance is bright white. On the contrary, once the air voids are removed by compression into solid ice, the scattering centers are lost and the appearance becomes transparent. Similar behavior was also observed in cellulose films: once the dimensions of the cellulose fibrils are brought down to nanoscale, transparent paper can be generated [70] or the optical properties (haze / transparency) of paper can be controlled for, e.g. solar cell applications [71].

Optical properties of traditional paper grades can be described in terms of opacity and whiteness in papermaking. Opacity measures the print visibility through the paper whereas whiteness measures the reflection at 457 nm. Kubelka-Munk parameters are phenomenological coefficients that relate the specific light scattering S and absorption coefficient K into reflection

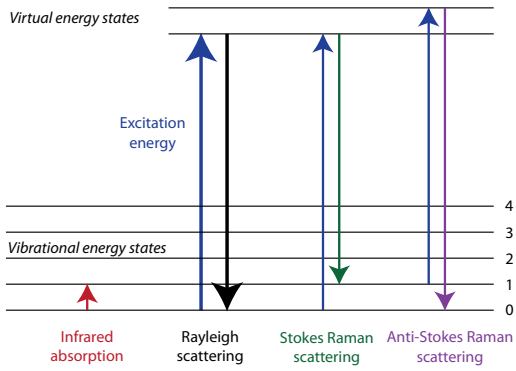

Figure 2.4: Generation of Raman scattering.

quantities R_0 and R_∞ that can be measured easily from a single paper sheet on top of a perfect absorber and a stack of paper sheets, respectively [72]. However, these parameters do not tell anything about the paper microstructure. For a more accurate numerical modeling, the discrete dipole approximation (DDA) was developed by Purcell and Pennypacker in 1973 [73]. The difficulty in DDA is the millions of individual dipoles that interact with each other requiring heavy numerical computations. This technique was originally developed for analyzing interstellar dust grains but it was recently extended to analyzing the optical properties of paper pigments and particles [74]. Scattering from nano- and microscale particles is typically called Mie scattering, and the scattering properties of an individual pigment particle can be calculated using Mie theory [75]. However, the significance of an individual scatterer analysis is of limited use for estimating the optical properties of pigment coated papers.

In addition to elastic scattering, inelastic scattering of photons was observed by C. V. Raman and K. S. Krishnan in 1928 [76] by photon energy up-conversion i.e. anti-Stokes shift in the energy that distinguished the new type of radiation from luminescence. The benefit of inelastic *Raman scattering* is that there is an interaction with molecules that scatter the light, typically with their vibrational energy states as shown in Fig. 2.4. Therefore, the Raman spectrum provides a unique fingerprint for each molecule allowing accurate and reliable identification of different substances. Compared to the traditional IR absorption spectroscopy that is based on detecting the change in the dipole moment caused by the IR radiation, Raman spectroscopy is based on the detection of induced dipole, i.e. the change of the polarizability of the molecule. This provides a significant benefit in analyzing aqueous solutions in which IR peaks of the molecules are blocked by the strong IR absorption of the water molecules whereas the Raman signal is significantly less sensitive to the presence of water molecules, and the Raman spectrum from aqueous solutions can easily be measured [77].

The most significant drawback of the Raman scattering is the very weak signal strength: elastic scattering is dominant with approximately only one photon in a million to ten million photons experiencing inelastic Raman scattering [77]. Therefore, Raman scattering is inherently weak by its nature, and the signal is easily lost, for example, in luminescence background. This would mean that very high concentration of the detected molecules would be required for reliable detection. Or alternatively one has to find ways to enhance the Raman signal intensity.

2.2.2 Surface-enhanced Raman scattering (SERS)

To enhance the Raman signal intensity several approaches have been taken. The first observation of extraordinary strong Raman scattering on a roughened metal surface was observed by Fleischmann et al. [78], related to the enhanced surface area of the rough surface. A few years later two groups independently observed anomalously large Raman intensities [79, 80] on roughened silver electrodes that displayed signal enhancement factors up to 10^5—10^6 far above the amount of increase in the surface area. However, the actual mechanisms of the signal enhancement in the surface-enhanced Raman scattering (SERS) was not fully understood. In principle, there are two possibilities for the signal enhancement: chemical or electromagnetic enhancement. The chemical enhancement is based on the metal-molecule charge transfer effects, and it has been confirmed that only an order of magnitude enhancement can be observed from these [81]. Hence, the electromagnetic enhancement plays the key role in the signal enhancement.

Typically electromagnetic enhancement is observed in metallic nanostructures, which support localized surface plasmon resonance (LSPR). The LSPR is a collective oscillation of electrons that induce a strong light localization in the vicinity of the metal nanostructures. This means that the metallic nanostructures act in a lens like manner, i.e. they concentrate the incoming light within a few nanometers of the nanostructure surface resulting in highly enhanced local electric field strengths. However, the local electric fields decay rapidly, and for small metal spheres the decay rate is r^{-10} [82]. Thus SERS only occurs when molecules are brought in the vicinity of the surface of such a SERS active substrate: SERS signal intensity depends on the fourth power of the local electric field strength and signal enhancement factors up to $10^{10} – 10^{11}$ have been reported [83].

Various nanostructures ranging from colloidal solutions to structures made by expensive electron beam lithography have been reported during the last decades [84]. Typically, the LSPR is observed in metal nanoparticles such as gold, silver, and copper that all have their plasmon resonance at visible wavelengths and are resistant to corrosion [82]. An additional benefit of the nanoparticles is that the optical response can easily be tailored from near-UV to mid-IR simply by changing the size and shape of the nanoparticles [85].

Theoretically a self-similar chain of silver nanoparticles was suggested to improve the enhancement, with electric enhancement factor up to 10^{13}, by a symmetric nanolens of six particles [86]. The idea was simple and elegant: by combining larger nanoparticles in the vicinity of smaller nanoparticles the electric field can effectively couple and cascade from a larger sphere into the smaller one. After cascading the electric field will also be squeezed into a smaller volume followed by an enlarged local electric field. Such a self-similar chain also avoided typical problems with small nanoparticles having a small optical cross-section that prevents effective excitation of the incident light. By cascading twice in a three particle (45 nm-15 nm-5 nm) self-similar chain, the electric field volume was effectively reduced. The theoretical proposal was verified a few years later by laser ablation of gold nanoparticles with SERS enhancement factors up to 10^9 [87]. For SERS hot spot generation both top-down and bottom-up approaches have been taken, see review [88]. These studies suggest that a random LFS deposition of silver nanoparticles could also be used for generating such hot spots on the surface [Paper II, Paper IV].

As a summary, SERS is a powerful, surface-sensitive, non-destructive, and in-situ vibrational spectroscopic technique that is suitable for detection of extremely low concentration molecules

[89]. Compared to fluorescence spectroscopy, Raman scattering is sensitive to different vibrational modes of the molecules and hence, provides a molecular fingerprint allowing detection down to a single molecule level [90,91] via enhancement of local electromagnetic fields. Since 2000 [92], tip-enhanced Raman spectroscopy (TERS) has been developed in which a sharp metal tip is used to excite local electric fields. This approach can result in simultaneous ultrahigh topographical imaging combined with quantitative Raman data. Several TERS set-ups have been developed from atomic force microscopy (AFM) to scanning tunneling microscope (STM) with various tip designs from antenna-structured tips to nanoparticle functionalized and etched metal tips [93].

SERS provides an accurate tool for detection of, for example, *Escherichia coli (E. coli)* bacteria [94], which is a major cause of foodborne illnesses. Increased threat of bioterrorism drives the interest in rapid and accurate detection of small amounts of pathogens down to single cell levels [95]. A handheld Raman spectrometer was recently demonstrated for identification of pathogens from human serum [96] that was incubated 3 h on commercially available silver nanorod substrates. Such an approach may provide quick diagnosis in remote locations with no microbiological laboratory access.

A typical problem with SERS active substrates is that the sample stains the used substrate. Hence, the SERS active material can only be used once. To avoid this problem, a combination of silver nanoparticles deposited on top of photocatalytically active TiO_2 nanorods was suggested [97,98]. The surface can be cleaned after the SERS analysis by exposure to UVA light that will photocatalytically degrade organic material from the substrate. Another possibility is to utilize SERS based sensoring on sustainable large-scale substrates that creates a need for low-cost disposable or recyclable SERS active substrates.

2.2.3 Developments of SERS on paper-based substrates

Over the past decade functional natural fibre based substrates have also found applications as disposable sensors. For example, bioactive paper is a promising candidate for inexpensive sensoring without any need for instrumentation [99] whereas printed planar reaction arrays can provide substantial cost savings in point-of-care diagnostics [100]. However, they are not suitable for detecting small amounts of pollutants, and hence, more accurate detection approaches are needed.

Several different approaches for low-cost substrates such as cellulose films and paper for SERS activation have been taken recently. For example, paper has been functionalized with plasmonic metal nanoparticles for SERS activity. Typically filter paper such as Whatman or chromatography paper has been used for the nanoparticle functionalization. As an example, gold nanorods were deposited by immersing paper substrate into the nanorod solution providing a rather uniform distribution of gold nanorods into paper [101]. An additional benefit of such nanorod functionalized paper is the possibility to swipe various surfaces for detection of trace elements such as explosives, narcotics, and pathogens. Alternatively, one can do the nanoparticle deposition directly on the cellulose fibers by reducing gold or silver from salt form into nanoparticles. For example, hydrogen tetrachloroaurate ($HAuCl_4 \cdot 3H_2O$) was used for gold nanoparticles [102] and silver nitrate ($AgNO_3$) was reduced to silver nanoparticles [103].

SERS active substrates were used for detection of antibodies with aptamer-functionalized gold nanoparticles and tyrosine in aqueous solution with silver nanoparticles, respectively. These

aptamer-functionalized gold nanoparticles can also be used for detection of cancer markers down nM level in the whole blood by SERS analysis on paper surface [104]. The sensivity can be enhanced by applying magnetic enrichment with novel principal component analysis (PCA) [105] for a more reliable separation of healthy and cancerous cell lines utilizing a cost-effective plasmonic paper. Sensitivity of SERS systems on paper of test molecules such as Rhodamine B (RhB) and crystal violet (CV) were shown to reach down to 10^{-11} M and 10^{-10} M, respectively [106]. Inkjet printed silver nanoparticles on cellulose were also shown to be suitable for SERS enhancement [107]. However, these results were obtained on a highly purified cellulose paper with specifically designed ink requiring several prints.

For inkjet printing, hydrophilic cellulose substrate is typically functionalized into a hydrophobically patterned and/or barrier surface. This prevents the deposited droplet from spreading and penetrating deep into the porous fibre network. Hence, for the surface to become functionalized with nanoparticles, significantly less noble metal nanoparticles are needed [108]. Furthermore, a hydrophobic surface provides a higher probability of forming a hot-spot of nanoparticles such as dimer, trimer, or quadrupole system of nanoparticles that can lead to a significantly higher SERS signal enhancement compared to an individual nanoparticle [109].

The interest in developing large-scale SERS active sensor platforms on paper-based substrates is based on several benefits: these substrates are renewable, recyclable, biodegradable, cost-efficient, and suitable for mass-production. In addition, SERS active structures can be printed on demand on the measurement site with no need for storage having sufficient accuracy and reproducibility for commercial use. The ultimate goal with such sensoring would be a combination of a handheld device, having the size of a smartphone without any need for laboratory environment.

Reproducibility of SERS active substrates and quantitative analysis remains a challenge for Raman spectroscopy. This is especially problematic in paper-based structures that are random, porous, and uneven. Several approaches have been taken to overcome this issue from surface sizing [110, 111] and using cellulose nanofibril for increased smoothness [112] to inverse opal carboxymethyl cellulose films [113]. A review article [114] summarizes the recent developments of cellulose-based substrates for SERS activity.

2.2.4 Photocatalytic activity of TiO_2

The word photocatalysis was introduced by M. Landau in 1912–1913 [115] covering the basic principle of heterogenous photocatalysis. The first observation of photocatalytic activity in TiO_2 was observed by Keidel in 1929 [116] as sunlight induced flaking of TiO_2 based paints with the photocatalytic degradation of the organic binder surrounding the pigment particles. Additionally TiO_2 was known to bleach the color of paints [117].

The work by Fujishima and Honda [12, 13] demonstrated that TiO_2 structures can be used with UVA light to break water molecules into hydrogen and oxygen. TiO_2 exists in three different crystalline forms: anatase, rutile, and brookite. There also exists an ultrahigh pressure crystalline form akaogiite [118]. The photocatalytical activity of different TiO_2 crystalline forms has been studied intensively, and it is still unclear which one has the highest activity [119–121].

In the LFS nanoparticle deposition of TiO_2 nanoparticles the main crystalline phase of the particles is anatase [122]. In another study, X-ray diffraction analysis showed that 86 wt.%

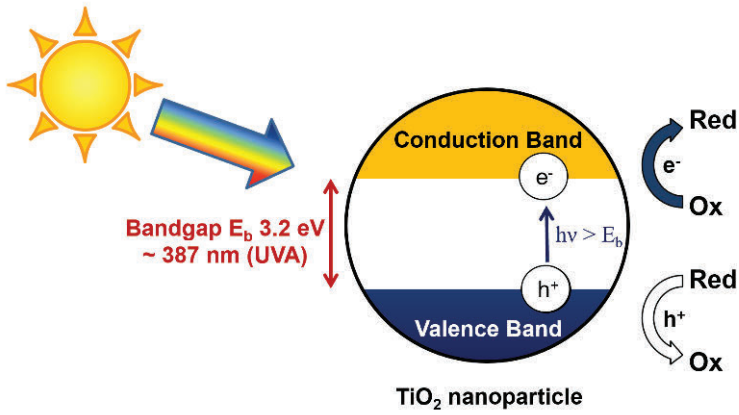

Figure 2.5: Photocatalytic activity of TiO_2 nanoparticles under UVA light exposure, leading to RedOx activity.

of the deposited nanoparticles had anatase crystalline form with an average crystallite size of 9.5 nm [63]. Anatase has a bandgap of 3.2 eV that corresponds to the UVA range at 387 nm. This means that UVA photons with higher energy (shorter wavelength) than the bandgap energy can excite electrons from the valence band into the conduction band of TiO_2, as illustrated in Figure 2.5. The electrons and holes can diffuse onto the surface of TiO_2, especially in nanostructures, on which they facilitate various reduction and oxidation (RedOx) reactions. These reactions can be used, for example, for photocatalytically induced superhydrophilicity and antifogging [123], antimicrobial activity [124, 125], and water splitting [126]. TiO_2 pigments are widely used in paints and photocatalytic activity can cause paint degradation upon UV exposure, for example, in art paintings [127]

A photocatalytically induced wettability change of TiO_2 surface was demonstrated around 20 years ago [128–130]. It has been shown that while deposited TiO_2 films are almost purely hydrophilic with water contact angle (WCA) close to 0°, the surface gets contaminated from the surrounding air increasing the WCA values up to 80° within a month [131]. Exposure to the UVA irradiation resulted in an increase of the OH groups on the surface lowering the contact angle close to zero. However, some organic compounds such as carboxyl groups can have a higher affinity onto the surface than water molecules [132]. Therefore, UVA irradiation can not completely remove all organic contaminants from the TiO_2 surface.

Controlled wettability of paperboard was demonstrated by using LFS deposited TiO_2 nanoparticles that can be converted from the superhydrophobic to highly hydrophilic state upon 30 min UVA irradiation [133]. The observed superhydrophobic nature of TiO_2 nanoparticles on paperboard is a unique feature as on other substrates such as aluminium, similar LFS deposition of TiO_2 resulted only in 83° WCA value [134]. Additionally, the observed superhydrophobicity on TiO_2 was contrary to the highly hydrophilic state of SiO_2 nanoparticle deposition [133]. Both TiO_2 and SiO_2 nanoparticles had a similar surface morphology but a different chemical composition was revealed by the XPS analysis, with the SiO_2 coating having a significantly higher

oxygen to carbon (O/C) ratio [67]. This was also in good agreement with the changes observed in the UVA activated wettability conversion of TiO_2 nanoparticles on paperboard [135] as UVA activation increases and heat treatment decreases the O/C ratio. Alternatively to external stimuli, controlled wettability from 10° to 160° can also be achieved by multicompound TiO_2-SiO_2 LFS deposited nanoparticles simply by controlling the ratio of elements in the precursor solution [53].

With TiO_2 nanoparticle coating, the UVA converted hydrophilic state is not permanent and the initial superhydrophobic state was recovered after 60 days storage in the dark. The recovery can be enhanced from months to minutes by heat treatment in an oven at 150°C [136]. The wettability conversion of LFS deposited TiO_2 nanoparticle coated paperboard with roll-to-roll stimulation methods showed that both corona and argon plasma treatment can be used to convert the surface to hydrophilic at up to 20 m/min web speed [137]. However, both corona and argon plasma induced hydrophilicity reverts to hydrophobicity within months similar to UVA conversion [138]. In addition, online hydrophobicity recovery was achieved with IR and UV illumination. The contradiction in the wetting behaviour by UV online exposure can be explained by the induced heat as surface temperature reached up to 140°C with the slowest web speeds, i.e. the heat treatment was dominant during the short exposure to the UV light.

In a recent paper [139] the role of surface adsorbates on a clean TiO_2 surface was studied using STM. It was shown that formic acid forms a monolayer on top of TiO_2 surface at ambient conditions, i.e. the formic acid effectively occupies the binding sites on the surface even at parts-per-billion concentration preventing adsorption of other species. This finding also explains the hydrophobicity recovery in dark conditions.

2.3 Paper

Paper is a random, porous, and continuous web of cellulose fibres that are bound together by hydrogen bonding between the cellulose molecules. Cellulose is the most abundant biopolymer on Earth, and typically the fibres for paper production are extracted from trees by chemical and/or mechanical treatment. The applications of paper products cover a wide range from graphic papers and technical papers to packaging of products with paperboard. The properties of a paper product can be adjusted upon the demands of the application, for example, by selection of the used fibre material and the extraction process, fillers, binders, additives, and end processing (coating, calendering, surface sizing) of the final product.

The history of papermaking dates back to ancient China, Ts'ai Lun being recorded as the inventor of paper at 105 AD [140]. For centuries individual sheets of paper were made in a similar fashion manually. In the early 19th century, the Fourdrinier brothers invented a papermachine with a flat, permeable wire (mesh) section that allowed for continuous roll-to-roll process flow. The first commercial Fourdrinier machine-made paper was manufactured already in 1812 [141]. The Fourdrinier machines have been the cornerstone in the growth of the paper and board industry: certainly significant developments have taken place in machine efficiency with increasing web speeds up to 2 000 m/min, web widths over 10 m, and novel automation. However, the basic principle of papermaking has changed little within the past 200 years.

Forest based products have been essential for the Finnish economy and society as forestry is one of the few natural resource generator available in Finland. Tar for wooden ships and ropes

was the first product for export, and Finland became a large exporter into the international tar market in the 16th and 17th century [142]. In the 1970s the Finnish paper manufacturers concentrated strongly on developing high-quality printing paper grades, and Finland became the world leading high-quality paper volume manufacturer in the 1980s. This resulted in a significant added-value to local economy. However, the paper companies were slow to react to the growth of electronic media and the challenges of the new millennium. The US market started the decline in the early 21st century, and in Finland 2006 marked the start of change with closures of several paper mills. Overcapacity in production, decline in the market demand, and increasing raw material and energy costs resulted in a market with low or no profitability, especially in certain light-weight coated (LWC) magazine paper grades. Now, 15 years later, the pulp and paper companies are in a much better financial shape, and even the paper production is profitable after significant restructuring of the industry. In 2019, 9.5 million tonnes of paper and board products were produced in Finland, and the forest products industry covers more than 20% of the export value from Finland [143].

2.3.1 Coating, calendering, and printing

Cellulose molecules have a high number of hydroxyl groups that makes the cellulose fibers inherently hydrophilic. In graphical arts applications, coated or uncoated paper is typically printed by offset lithography, rotogravure, flexography or inkjet printing. For improved print quality, several technologies have been developed during the past century ranging from coating concepts to surface sizing and calendering. The print quality is evaluated with parameters such as color gamut and print density, evenness (free of mottling), opacity, gloss and image sharpness [144].

In dispersion coating a slurry of pigments such as kaolin, talc, or calcium carbonate is applied on top of cellulose fibers as a suspension containing binder, for example, styrene-acrylic (SA) or styrene-butadiene (SB) latex or starch [145]. The mineral pigment particles can be used either as fillers in base paper or in coatings to improve both surface smoothness and optical properties of papers by increasing the number of scattering centers. Optimizing the size and number of scattering units allows thinner coatings to have sufficient optical properties for reduced cost, and inspiration from natural white pigments found in a beetle *Cyphochilus* spp. have been utilized [35, 146]. Additives such as optical brightening agents (OBAs) or high refractive index TiO_2 pigments can be added to the sizing and coating formulations to improve the brightness, whiteness and opacity of the paper.

Surface sizing is typically carried out using starch, carboxy methyl cellulose, polyvinyl alcohol or a synthetic polymer to increase the strength and to reduce liquid absorption and permeation into paper [145]. Typically, surface sizing is applied to uncoated papers such as copy papers for improved print quality in inkjet and laser printing. Closing of the surface with surface sizing is especially important in paper-based SERS substrates as metallic nanoparticles would otherwise penetrate deep into the paper substrate whereas they should be on the surface to provide the best possible enhancement [110]. In addition, surface sizing prevents the tested molecules from penetrating into the base paper as the SERS enhancement requires a close vicinity of the molecules to metal nanoparticles [107].

Several concepts for paper coating exist from traditional blade coating to recently developed curtain coating technologies. A wet coating layer applied on top of base paper consolidates and

forms a porous dry pigment coating layer. Surface smoothness can be improved by soft-nip or hard-nip calendering of the base paper as well as the coated paper. All these tools have a significant effect on porosity, printability, and ink setting properties of the final paper product. Additionally, both interparticle and intraparticle porosity can be tuned by choice of pigments. Porous $CaCO_3$ pigments [147] have also found applications in the food industry [148].

Since 2000 printed electronics and functionality such as flexible displays, radio-frequency identification (RFID) labels, and anti-counterfeiting on banknotes [149] have been subjects of intensive research. The first demonstration of solar cells on paper was carried out in 2011 by two different approaches: a perfect contour coating by oxidative chemical vapor deposition prevented formation of electronic shorts [150], whereas an all-printed solution was based on the use of smooth transfer foil that reduced paper roughness [151]. A recent review [152] summarizes the developments of the past decade with printed solar cells on paper.

The possibility for all roll-to-roll process flow can yield significant reduction in the production cost [153]. Traditionally, functional applications have been realized on plastic substrates but demands for sustainability have made renewable, cellulose based solutions desirable [154]. However, paper is rough, porous, and hydrophilic in nature, and specific coatings are needed for functional applications. A multilayer coated paper for printed electronics combined a sealing layer with porous top layer that allowed tailorable ink setting properties [155]. In addition to sustainability and tailorability, cellulose-based substrates are also significantly more cost-effective than plastic or glass substrates [156].

2.3.2 Wetting

The behaviour of liquids on solid surfaces is a well known phenomenon for all of us. During rain, umbrellas are used, and wipers for the windscreens in cars, and coffee spilled on a surface leaves a round-like stain [157]. On smooth, solid surface liquid forms a sessile drop having a *contact angle* with the surface. Water is typically applied on the surface to characterize whether the surface is *hydrophilic* or *hydrophobic*. For hydrophilic surfaces the contact angles are less than 90° and water wets the surface. For hydrophobic surfaces water forms discrete droplets.

Nature has found many ways to utilize the peculiar properties of water. A beetle species *Stecanora sp.* collects its drinking water from morning fog in the Namib desert by tilting its body towards the wind [158]. A microstructure on the back of the beetle extracts large droplets of wa-

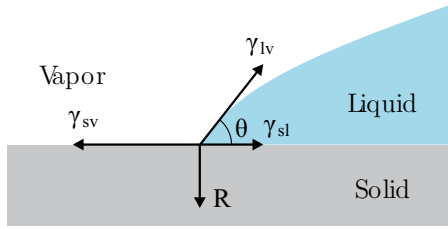

Figure 2.6: A liquid drop on a solid flat surface: in practice, the vapor may often be replaced by another liquid.

ter from fog that are collected. Certain fishing spider species utilize hydrophobicity for aquatic motion: the contact angles up to 150° in the hairs of their body allow moving on the surfaces of ponds and streams [159]. Similar *superhydrophobicity* is found at the surface of Lotus leaves having contact angles up to 160°, i.e. water droplets are repelled by the structure and slide out from the leaves. This effect has been characterized in detail using SEM [160, 161]. Superhydrophobicity is caused by both chemical and physical effects of the surface. For flat surfaces the highest contact angles have been observed with regularly aligned and hexagonal packed fluorinated -CF_3 groups displaying an angle of 119° [162]. Thus the *surface morphology* plays an essential role in superhydrophobicity.

The theoretical investigation of liquid behaviour on a solid surface dates back to the start of the 19th century and to the works of Thomas Young. The macroscopic concept of contact angle was introduced by Young as he considered the forces acting on a droplet on a smooth, solid surface [163]. Within the past two centuries the concepts of wetting have been developed: the macroscopic hydrodynamic calculations and molecular dynamic simulations are finally converging [164]. Here various models used in describing wetting phenomena are reviewed.

For a liquid spreading on a flat surface shown in Fig. 2.6, the surface energies (for an infinitesimal unit length dz of the contact line) are modified by the amount dE as follows:

$$\mathrm{d}E = (\gamma_{\mathrm{sl}} - \gamma_{\mathrm{sv}})\mathrm{d}z + \gamma_{\mathrm{lv}} \cos\theta \mathrm{d}z. \tag{2.4}$$

Here γ_{sl}, γ_{sv}, and γ_{lv} are the surface tensions between solid-vapor, solid-liquid, and liquid-vapor interfaces, and θ is the contact angle at the three-phase line. In Eq. (2.4) the first term corresponds to the dry solid replaced by a wet one. The second term is caused by the creation of liquid-vapor interface as the drop spreads. In equilibrium, the Young's equation for the contact angle is

$$\cos\theta = \frac{\gamma_{\mathrm{sv}} - \gamma_{\mathrm{sl}}}{\gamma_{\mathrm{lv}}}. \tag{2.5}$$

From the Young's equation the following conditions can be observed:

1. The surface is hydrophobic when $\gamma_{\mathrm{sl}} \geq \gamma_{\mathrm{sv}}$ and $\cos\theta \leq 0$.

2. Wetting is observed when $\gamma_{\mathrm{sv}} - \gamma_{\mathrm{sl}} \geq \gamma_{\mathrm{lv}}$ and $0 < \cos\theta < 1$. Silicone oil with low surface tension satisfies this condition on many substrates such as glass, steel or plastics [165].

3. A non-wetting situation is observed when $\gamma_{\mathrm{sl}} - \gamma_{\mathrm{sv}} \geq \gamma_{\mathrm{lv}}$ and $-1 < \cos\theta < 0$. Fully superhydrophobic surface with $\theta = 180°$ was realized by using organosilanes on a *rough microstructured* surface [166] .

Alternative derivations for the Young's equation can be done, for example, by using simple geometry for balancing the forces or by applying Lagrangian mechanics. The surface forces normal to the surface are balanced by the resistance of the solid [167].

The Young's theory is only valid for flat, smooth surfaces. For rough surfaces several different approaches have been developed. Wenzel [168] considered a wetting rough surface with a geometrical roughness parameter that changes the Young's case as follows:

$$\mathrm{d}E = r(\gamma_{\mathrm{sl}} - \gamma_{\mathrm{sv}})\mathrm{d}z + \gamma_{\mathrm{lv}} \cos\theta_{\mathrm{W}} \mathrm{d}z, \tag{2.6}$$

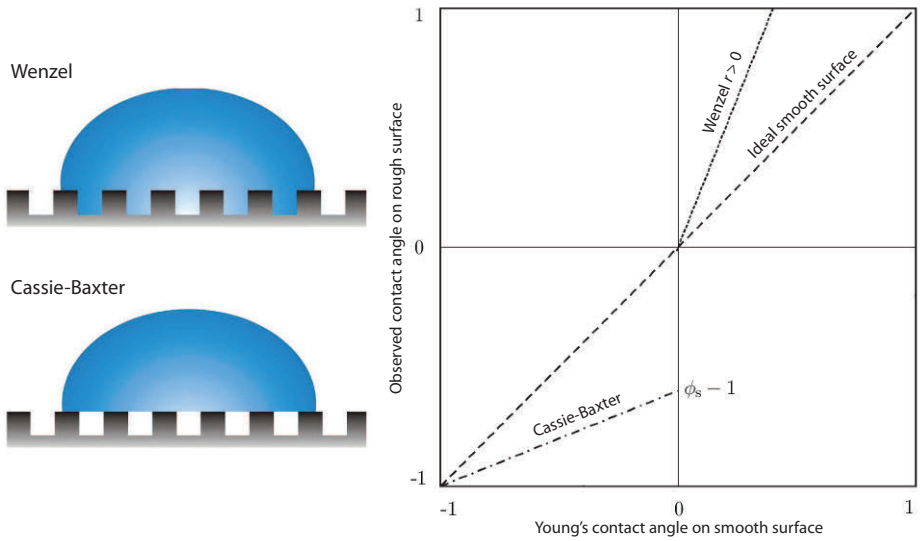

Figure 2.7: Schematic figure of Wenzel and Cassie-Baxter states with the corresponding curvatures.

where the roughness parameter $r > 1$ is the ratio of the actual surface area to the projected one. In equilibrium one ends up with the Wenzel model for a wetting rough surface:

$$\cos\theta_{\mathrm{W}} = r\cos\theta_{\mathrm{flat}}, \tag{2.7}$$

where θ_{W} is termed the Wenzel contact angle, representing the effective observed value, and θ_{flat} the contact angle that would be made upon contact with a perfectly flat surface of the same material.

For a hydrophobic rough surface Cassie-Baxter [169] model is typically used. In this case, a water drop rests on a surface formed by solid with air pockets. Hence, the energy equation (2.4) can be written in the form [170]:

$$\mathrm{d}E = \phi_{\mathrm{s}}(\gamma_{\mathrm{sl}} - \gamma_{\mathrm{sv}})\mathrm{d}z + (1-\phi_{\mathrm{s}})\gamma_{\mathrm{lv}}\mathrm{d}z + \gamma_{\mathrm{lv}}\cos\theta_{\mathrm{CB}}\mathrm{d}z, \tag{2.8}$$

where ϕ_{s} is the solid fraction of the surface. At equilibrium, a Cassie-Baxter equation is observed:

$$\cos\theta_{\mathrm{CB}} = \phi_{\mathrm{s}}(\cos\theta_{\mathrm{flat}} + 1) - 1, \tag{2.9}$$

where θ_{CB} here refers to the Cassie-Baxter contact angle, representing the effective observed value, and, once again, θ_{flat} the contact angle that would be made upon contact with a perfectly flat surface of the same material.

Figure 2.7 summarizes the differences in Wenzel and Cassie-Baxter states. Experimental study with fractal surfaces confirmed these observations from theoretical models [171, 172]. Superhydrophobic surfaces are typically observed in hierarchical structures combining micro- and nanoscale features. It is noteworthy that under forced wetting, i.e. by applying external pressure dynamic wetting can take place even on a hydrophobic surface [173, 174]. Forced wetting

typically occurs in engineering applications such as in offset printing. Nanostructured surfaces have found a large number of applications in recent years ranging from slippery liquid infused porous surfaces (SLIPS) [175] and superamphiphobic surfaces [176,177] to icephobic superhydrophobic [178] and SLIPS surfaces [179].

Hierarchical structures are typically weak in their nature. For example, both wear [180] and compression [Paper I] were studied on LFS deposited TiO_2 nanoparticle surface: the superhydrophobicity was lost in both cases. On a rough surface with small contact area the local mechanical stresses can be high. Various designs for protecting the sensitive micro- and nanoscale textured surface have been developed from micropillars [181] to microstructure armour on metal, glass, and ceramic surfaces [182].

Superhydrophobic surfaces can also display a petal effect when a surface has both high contact angle and high adhesion of water. High adhesion is observed with a large contact angle hysteresis, i.e. a large difference between the advancing and receding contact angles [183]. In addition to static contact angle, dynamic contact angle describes the velocity dependent contact angles that may differ significantly from the static one even at low droplet velocities [184]. The dynamics of contact angle are especially important in microfluidic applications.

2.3.3 Microfluidics on paper

The seminal work in microfluidics was carried out by Terry et al. in 1979 [185] who reduced the size of conventional gas chromatography by three orders of magnitude by etching microstructures on a silicon wafer. Nowadays microfluidic devices are used routinely, for example, from DNA sequencing and genotyping [186] to microfluidic enzyme-linked immunosorbent assays (ELISA) [187, 188]. Typically lab-on-chip type microfluidic devices are realized on silicon, glass, or polydimethylsiloxane (PDMS) substrates having complex nano- and microscale designs [189], but a more cost-efficient alternative to such substrates has remained an important goal.

The first fluidic channel on paper was demonstrated already in 1949 [190] by patterning a filter paper by paraffin wax barrier for liquid chromatography purposes. Microfluidic designs were expanded to paper-based substrates in 2007 by Whitesides' group [191, 192] that was based on a three-dimensional hydrophilic paper structure patterned with a hydrophobic wax or PDMS polymer. A high potential for paper based microfluidic devices is expected in developing countries with simple detection, for example, by colorimetry. Colorimetric change can easily be evaluated by visual or mobile phone technology [193] that can have a significant contribution to public health. Microfluidic devices on paper platform have also found applications as cell culture platforms [194].

Liquid flow in paper based systems is governed by capillary wicking into the porous fibre network. A typical problem with commercial coated and surface sized papers is inadequate and slow wicking due to the pore structure. Recently functionalized porous $CaCO_3$ based coating concepts have been developed [195, 196] that allow a rapid wicking with controllable intra- and interparticle porosity.

Alternatively, microfluidics can be performed on top of a hydrophobic paper. A paperboard surface functionalized with LFS deposited TiO_2 nanoparticles was demonstrated for planar microfluidics [197] in which a photomask was used for generating UVA activated wettable chan-

nels onto an otherwise superhydrophobic surface. It was also shown that liquid flow velocity can simply be controlled by the exposed channel width [198]. However, the reversion of the UVA activated areas within 60 days after the illumination limits the shelf lifetime of the fabricated structures. Mechanical durability of plasma etched hierarchical structures on polymethylmethacrylate (PMMA) substrates was studied under successive wetting- drying cycles [199]. It was shown that the nanostructured surface coalesced under wetting with a significant and permanent change in the surface morphology. A similar approach was taken in this thesis [Paper III] by exposing the UVA illuminated area to water that converted the channel area to being permanently hydrophilic.

2.3.4 Modified atmosphere packages (MAPs)

Modified atmosphere packages (MAPs) were developed to extend the packaged product shelf lifetime by replacing the regular atmosphere by nitrogen, carbon dioxide, oxygen, or a controlled mixture of these gases according to the demands of the packaged product. CO_2 is known for reducing growth of bacteria and fungi, and reduced oxygen content decreases the growth of aerobic bacteria [200]. It is estimated that up to one third of the food produced today is wasted with a direct economic cost of up to 705 billion USD annually [201]. Food-borne pathogens are also severe issue and in the United States alone they contribute to more than 300 000 hospitalizations annually [202].

Modified atmosphere was used for the first time in the 1920s in the storage of apples that remained fresh for a longer time in an increased CO_2 atmosphere. The first MAPs were brought to the market in 1979 by Marks and Spencer [203], whereas in North America the first application of MAPs for fresh-cut products was in lettuce packages by McDonald's [204]. Today the market value of MAPs is estimated to be around 13 billion USD in 2019 [205].

Functional printing for intelligent MAPs is undergoing growing interest as it can yield information about the product quality during handling, transportation, and storage. Several approaches have been taken for the development of oxygen indicators from luminescence [206] and electrochemical [207] to colorimetric detection by intelligent inks for oxygen [208, 209]. Typically the intelligent oxygen inks are based on methylene blue (MB) that is a heterocyclic aromatic chemical compound being a cationic dye with maximum light absorption around 670 nm in an oxidized form [210]. In the reduced *leuco* form (LMB) the absorption peak vanishes and the dye is transparent. The photoreduction can be carried out by UVA excitation of the TiO_2 component that can be on the surface or mixed as particles in the solution. The color conversion is reversible as LMB quickly regains the initial MB blue shade once exposed to oxygen. Inkjet printed oxygen indicators with solvent-based MB formulation have been realized [211]. However, large scale utilization of a roll-to-roll process flow would be beneficial for reduced cost that could be realized with flexographic printing. In addition, a surface fully coated with functional inks can be combined with a patterned photomask, and so, when selectively exposed to chosen light wavelength(s), could thus enable various designs to be made for applications, such as labels and safety features, as discussed in this thesis [Paper V].

Chapter 3

Materials and Methods

The materials and methods summarizes the main aspects of the used substrates and nanoparticles for the three applications studied in this thesis complemented with the used characterization techniques. More details of the experiments are given in attached Papers I–V.

3.1 Substrates

A commercial double pigment coated paperboard (200 g/m^2, Natura, Stora Enso, Skoghall, Sweden) was used in Papers I, III , and IV. A cross-sectional image of the paperboard is presented in Fig. 3.1. The thickness of the paperboard is approximately 300 µm. The top 20 µm is formed by a double pigment coating that reduces surface roughness and porosity for improved print quality.

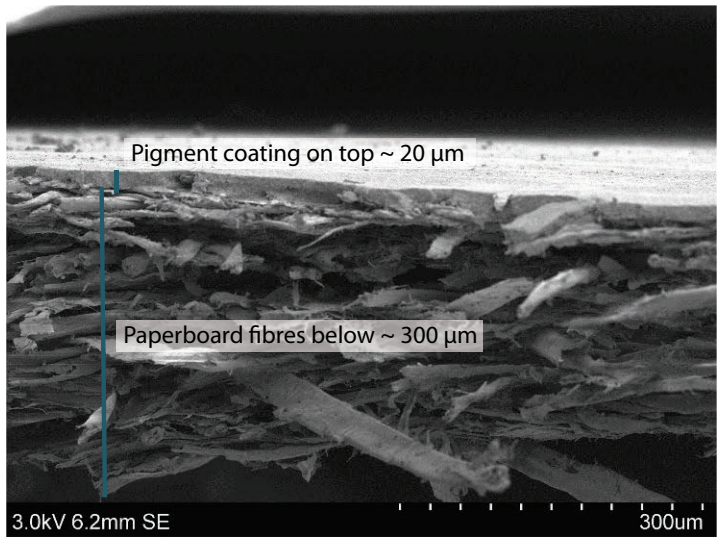

Figure 3.1: Cross-sectional image of double pigment coated paperboard

Commercial microscope glass (Menzel Gläser, DE) was used as a substrate for AgNP deposition for SERS active substrates in Paper II.

A specifically designed multilayer paper for printed electronics [155] was used in Paper V for flexographic printing of oxygen indicator ink. Additionally commercial poly(ethylene terephtalate) (PET) plastic film (Mylar® A, Dupont, US) was used as a reference.

3.2 Nanoparticles

3.2.1 Silver nanoparticles deposited by liquid flame spray (LFS)

Two different sized silver nanoparticles (AgNPs) were deposited both on glass and paperboard substrates by LFS. Silver nitrate ($AgNO_3$, $> 99.9\%$ purity, Alfa Aesar) dissolved in water was used as a precursor for AgNPs in Papers II and IV. For 50 nm diameter AgNPs the precursor was fed with a rate of 4 ml/min and concentration of 750 mg/ml into the flame that was formed with hydrogen and oxygen flow of 55 l/min and 5 l/min, respectively. For 90 nm diameter AgNPs the corresponding parameters were 2 ml/min and 500 mg/ml with 40 l/min (O_2) and 20 l/min (H_2).

AgNPs were deposited using both direct and indirect deposition methods. Direct deposition was carried out using a rotating carousel in which the deposited nanoparticle amount was controlled simply by the number of times the substrate passes through the flame (sweeps). The indirect method was performed with the aid of a deposition tube, i.e. the AgNPs were transferred along the tube onto the adjacent substrate, and the coating amount was controlled by the deposition time that the substrate resided at the end of the tube.

3.2.2 TiO_2 nanoparticles by LFS

TiO_2 nanoparticles (TiO_2NPs) in Papers I and III were deposited using titanium tetraisopropoxide (TTIP, 97% purity, Sigma Aldrich) precursor dissolved in isopropanol (IPA) with a metal ion concentration of 50 mg/ml. 12 ml/min of precursor was fed into the flame with gas flow rates of 15 l/min (O_2) and 50 l/min (H_2). TiO_2NPs were deposited on a paperboard in roll-to-roll deposition using the converting pilot line at the Tampere University of Technology (Finland). Paperboard web speed was set to 50 m/min and the burner distance to the paperboard surface was set to 6 cm.

3.2.3 Commercial TiO_2 nanoparticles for colorimetric ink

Commercial TiO_2NPs in anatase crystalline form (E171, Sigma Aldrich) were utilized together with methylene blue (MB, Sigma Aldrich) dye for colorimetric ink in Paper V. MB, TiO_2NPs, and glycerol (Sigma Aldrich) in water or ethanol were mixed with a magnetic stirrer. The colorimetric ink was used both in reverse gravure (RG) coating and flexographic printing. For coating, the ink was diluted to 2 wt% with a ratio of 1:6:2 for MB:TiO_2NPs:glycerol dissolved in ethanol. For flexography, the viscosity of the ink was increased by increasing concentration to 5 wt% with a ratio of 1:10:4 for MB:TiO_2NPs:glycerol and adding ethylene glycol (Sigma Aldrich).

3.3 Coating, calendering, and printing

3.3.1 Reverse gravure (RG) coating

RG coating in Paper V was carried out using a MiniLabo test coater (Yasui Seiki, US). In RG, a microgravure (anilox) roll rotating against the web in the counter (reverse) direction is utilized to transfer coating from the coating pan. A doctor blade is utilized to remove the excess coating from the microgravure roll. A trihelical gravure roll having a diameter of 2 cm with 80 lines/inch (31.5 lines/cm) was used for uniform coating. The web speed was set to 1.0–1.6 m/min and roll surface speed to 1.9 m/min. These settings resulted in a 15 µm wet film thickness that corresponds to a dry film thickness of 100 nm with 0.7 vol%.

3.3.2 Calendering

Calendering is a mechanical compressive surface treatment and finishing technology to improve smoothness and optical properties of papers, textiles, and polymers. Several different technologies exist with multiple rolls and roll materials forming the compression nip through which the web is fed. In Paper I a DT Laboratory Calender with soft/hard roll (DT Paper Science, FI) was used to study the compressibility and smoothness of LFS TiO_2NP coated paperboard. A roll temperature of 60°C with a line load of 104 kN/m was utilized. The LFS deposited TiO_2NP functionalized paperboard surface was always facing the hard steel roll to prevent NP transfer onto the soft polymer roll. The same parameters were used in successive calendering runs.

3.3.3 Flexography

Flexographic printing was utilized in Papers IV and V. In Paper IV, the protective carbon coating by graphite ink on paperboard for the SERS measurements was carried using a laboratory scale flexography printer (IGT GST 2 printability tester, IGT Testing Systems, NL) with a graphite ink (110-04, Creative Materials, US). The anilox had 40 lines/cm with a 45° cell angle and 20 ml/m^2 cell volume. A printing speed of 1.0 m/s was used for the successive graphite ink print runs. The pressure between the anilox cylinder and the printing plate, and between the printing plate and substrate, were set to 50 N and 100 N, respectively.

A custom-built, roll-to-roll mini pilot scale hybrid printer (Åbo Akademi FunPrinter) was used in Paper V with functional methylene blue-TiO_2NP ink. Several different designs for oxygen indicators were printed on both commercial plastic film (Mylar® A) and multilayer coated paper [155]. A web width of 10–12 cm was used with printing speed of 10 m/min with two infrared drying units (500 W, HQE 500, Ceramics) that were placed 15 cm after the printing nip with a distance of 3 cm from the substrate. The used ceramic anilox roll (Cheshire Anilox Technology, UK) had a cell angle of 60° with cell volume and line density of 17.2 cm^3/m^2 and 118.7 lines/cm, respectively.

3.3.4 Inkjet printing

A laboratory scale piezoelectric inkjet printer Dimatix DMP-2800 (Fujifilm Dimatix, US) was used in Papers II and IV for printing silver ink on glass and paperboard substrates. Commercial

silver ink U5603 (Sun Chemicals, US) with AgNPs in the size range from 20 to 50 nm dispersed in ethanol, ethylene glycol, and glycerol was used. Drop volume of 10 pl was utilized with drop spacing (DS) values of 45, 60, and 85 µm. A 45 µm DS value resulted in a rather uniform silver coverage on the substrate. The inkjet printed samples were cured in an oven at 120°C for 30 min to guarantee ink setting on the substrate. Additionally a 200°C curing temperature was also tested but the higher curing temperature resulted in a SERS non-active substrate.

3.4 Ultraviolet A (UVA) activation

Ultraviolet A (UVA, 315–380 nm) radiation was used in Papers I, III, and V. The high intensity UVA source used was a Bluepoint 4 (Hönle UV Technology, DE) with a 150 W mercury lamp (365 nm central wavelength). The UVA emission was ensured using a bandpass filter of 320–390 nm. For controlled wettability studies with TiO_2NPs on paperboard (Papers I and III), a constant intensity of 50 mW/cm^2 was applied for 30 min. A low intensity UVA source LV202-E (Mega Electronics, US) with two 8 W fluorescent bulbs was used in Paper V that resulted in approximately 2 mW/cm^2 intensity. The power spectrum and total intensity were recorded using an Ocean Optics USB2000+ miniature optic fiber spectrometer and a FieldMaster GC laser power and energy meter (Coherent, US), respectively.

3.5 Physico-chemical characterization

Several different tools were used to study the physico-chemical properties of the nanoparticle functionalized surfaces. Figure 3.2 summarizes the schematics of the three main techniques used in this thesis.

3.5.1 Scanning electron microscopy (SEM)

SEM utilizes a high intensity electron beam that is scanned pixel-by-pixel over the sample surface. For a high quality and narrow beam, ultrahigh vacuum (UHV) is required as molecules and dust particles would interfere with the electron beam. Traditionally, tungsten filaments have been used as electron sources, but, more recently, field emission SEMs (FESEMs) have replaced

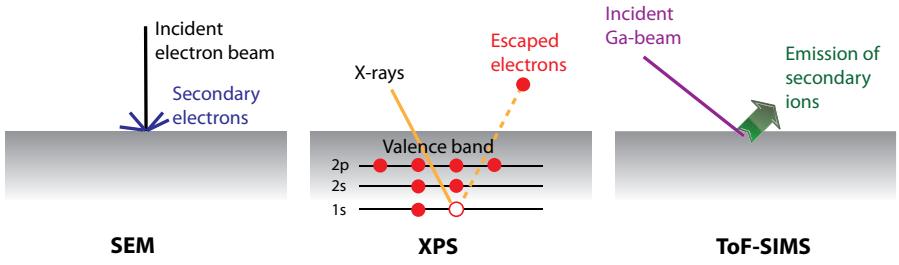

Figure 3.2: Schematics of SEM, XPS, and ToF-SIMS characterization techniques.

the traditional ones with significantly improved beam quality, and thus better image resolution. Nowadays the best FESEMs have spatial resolution down to a few nm with accelerating voltages up to 300 kV.

The incident electrons interact with the atoms of the sample, and experience either elastic or inelastic scattering. Secondary electron (SE) imaging is the most used analysis mode in SEM that is based on inelastic scattering, and the image contrast is formed by the intensity of the emitted SE. In contrast, back-scattered electrons (BSE) experience elastic scattering. Therefore, SE yield the highest topographical imaging and the BSE signal can be used to distinguish different elements on the surface as heavier elements have a larger interaction with the incident beam.

Typically SEM imaging requires conductive samples to prevent charging of the surface caused by the incident electron flux. Traditionally, non-conductive samples are sputtered by a few nm thick layer of gold or platinum for conductivity.

Several different FESEM devices were used during this study. In Paper I, an SU 6600 (Hitachi, JP), and, in Paper III, a Leo Gemini 1530 (Zeiss, DE) were used with an in-lens detector. The TiO_2NP samples were carbon coated before imaging for conductivity, and magnification from 5 kX to 50 kX was used. The accelerating voltage was set to 27 kV with a working distance of 4–5 mm. In Papers II and IV, a Carl Zeiss Ultra-55 FESEM (Carl Zeiss, DE) was used with both SE detector and energy and angle selective backscattered electron (ESB) detector. ESB provides accurate compositional information about the sample surface. With the Ultra-55, the accelerating voltage and magnifation were set to 1.0 kV and 10 kX, respectively. An energy window of 482 eV was set to perform ESB analysis to prevent SE detection in the BSE detector, thus improving the compositional contrast.

3.5.2 X-ray photoelectron spectroscopy (XPS)

The theoretical background of XPS lies in the Nobel prize work by Albert Einstein on the photoelectric effect. In XPS, high energy photons hit the sample surface and emit electrons. XPS utilizes X-rays to excite electrons which become emitted from the investigated material. The used X-rays can penetrate deep into the sample but the photoemitted electrons are quickly dissipated by the neighboring atoms. This guarantees the high surface sensitivity of XPS devices down to 10 nm.

Different elements have different binding energies for the emitted electrons. Hence, simply by measuring the kinetic energy (KE) of the emitted photoelectrons one can easily calculate the corresponding binding energy (BE) with a known energy for the used radiation. This is given by

$$\mathrm{BE} = h\nu - \mathrm{KE} - \phi_{\mathrm{spec}}, \tag{3.1}$$

where h is the Planck's constant, ν the frequency of the used X-ray source, and ϕ_{spec} the spectrometer work function. The observed energies and peak shapes can be compared to manuals [212], which contain XPS peak values for different elements measured from pure compounds.

XPS measurements in Papers II, III, and IV were performed using a PHI Quantum 2000 device (Physical Electronics, US). A monochromatic Al Kα X-ray source, operating at 25 W, was used to emit the surface electrons with a take-off angle of 45° relative to the sample surface.

Ultrahigh vacuum of 2×10^{-7} Torr was used. Two different pass energies were employed: for AgNPs in Papers II and IV, 184 eV was used for survey analysis, whereas, for TiO_2NPs in Paper III, 29.35 eV was used for high resolution spectra acquisition. Three different spots were measured, each approximately 100 µm in diameter. A mixed Gaussian-Lorentzian curve fitting was carried out together with Shirley background reduction [213].

3.5.3 Time-of-flight secondary ion mass spectroscopy (ToF-SIMS)

ToF-SIMS is a highly surface sensitive characterization tool down to a few nm from the sample surface. The sample surface is bombarded with a primary ion beam, and the extracted secondary ions are separated using the difference in their time-of-flight. The primary ion beam source is typically a liquid metal ion gun with three possible ion sources: Ga, Au, and Bi. In Paper III the TiO_2NP coated paperboard was measured using PHI Trift II (Physical Electronics, US) with a Ga ion source. A mass range from 2 to 2 000 Da was measured over a 10 min acquisition time with a raster size of 100×100 µm^2, 15 kV applied voltage, and 600 pA aperture current. Non-interlaced mode was used with sputtering and analysis performed during different ToF cycles.

3.5.4 Raman spectroscopy

Raman spectra AgNPs functionalized with a crystal violet (CV) sample analyte were recorded in Papers II and IV using a Shamrock 303 spectrometer (Andor Technology, UK) with a Newton 940P CCD camera (Andor Technology, UK). The Raman excitation was carried out by a diode pumped solid state laser (Cobolt Samba, Hübner Photonics, DE) with 532 nm wavelength. The collimated laser beam was guided to the sample surface at an angle of 30° whereas the scattered light was collected through a microscope objective along the normal of the sample surface. Rayleigh scattering was excluded from the signal by RazorEdge filter (Semrock, US). The used spot size was approximately 700 µm in diameter on the sample surface.

3.5.5 Surface wettability

Water contact angles (WCAs) were measured in Papers I and III using a KSV CAM 200 contact angle goniometer (Biolin Scientific, FI) with an automatic dispenser on a motorized stage. Two water droplet volumes were used: in Paper I a 2 µl was placed on the sample surface whereas in Paper III approximately 6 µl volume was used. The formed droplets were recorded by a digital camera with a 55 mm zoom microscope lens. The results were analyzed using the KSV CAM software with a Laplacian fit to the droplet curvature, and the standard deviation for the measured WCA was approximately $\pm 3°$. At least three parallel measurements were carried out for each sample.

Chapter 4

Results

The results section is divided into three parts. First, controlled wettability and formation of permanent planar fluidic channels were demonstrated in Papers I and III. Secondly, SERS active substrates on renewable cellulose based substrates were developed in Papers II and IV. Finally, coatable and printable oxygen indicators were studied in Paper V for modified atmosphere packages.

4.1 Controlled wettability

4.1.1 Controlled wettability by UVA activation and controlled roughness

In Paper I the effect of surface roughness and UVA activation were studied on TiO_2NP coated paperboard. TiO_2NPs deposited by LFS on a paperboard surface have been demonstrated to induce a superhydrophobic surface (WCA up to 161°) [56, 66, 133]. This was contrary to the findings with TiO_2NP depositions on Al foil [67] on which TiO_2NP induced a WCA of 83°. Since the pure TiO_2 surfaces are completely hydrophilic (WCA close to 0°) [131], it is presumed that the heat from the flame during the LFS deposition can evaporate volatile organic compounds from the paperboard that are then covering the deposited nanoparticles.

Figure 4.1 shows the cross-sectional SEM imaging of the calendered TiO_2NP coated paperboard samples, and summarizes the effect of calendering on surface roughness as a function of successive passes through the calendering nip. It is evident that even a single pass significantly reduces surface roughness. Superhydrophobic surfaces require both hydrophobic chemistry and suitable roughness to increase the WCA values over 150°. The findings with a highly porous network of TiO_2NPs are in agreement with literature, where LFS NPs have been found to form a highly porous network on the substrate surface with porosity up to 98% [58].

The roughness values of the corresponding samples were also measured using an AFM in tapping mode from 100×100 μm^2 and 20×20 μm^2 areas. The greatest decrease was observed for the TiO_2NP coated paperboard after the first pass through calender nip as roughness values were reduced by more than 50%.

The corresponding WCA values for the reference paperboard and for TiO_2NP coated paper-

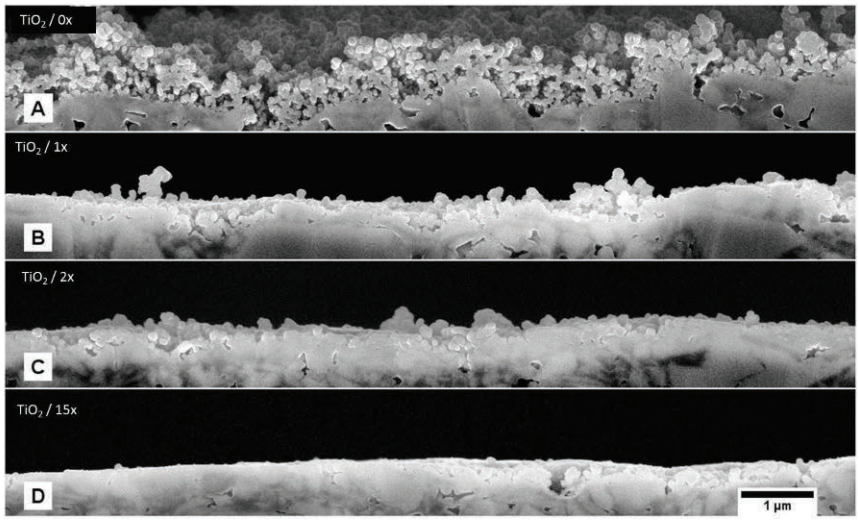

Figure 4.1: Cross-sectional SEM images of TiO_2NP coated paperboard as a function of successive calendering passes: A) Uncalendered, B) 1 pass, C) 2 passes, and D) 15 passes. [Paper I]

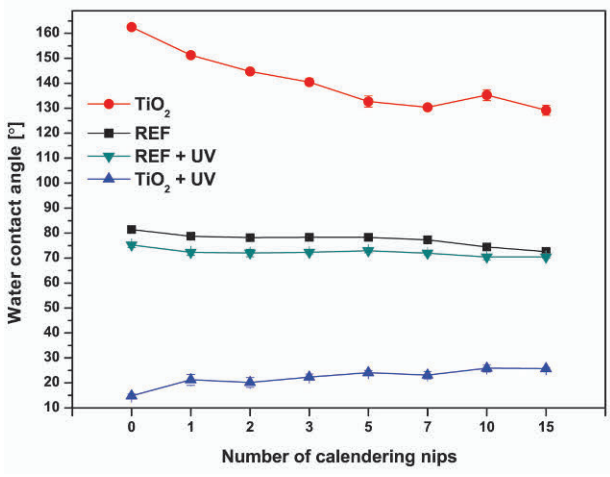

Figure 4.2: WCA values of the reference paperboard and TiO_2NP coated paperboard as a function of successive calendering passes. [Paper I]

board are presented in Fig. 4.2. The reference paperboard had an initial WCA value of approximately 80° that remained almost constant independent of calendering. Similarly, the UVA treatment did not have a significant effect on the wettability of the reference paperboard. On the contrary, the TiO_2NP coated paperboard displayed initial contact angle values greater than

160° that were reduced to 130° level as the number of successive calendering passes was increased to 15. Additionally TiO_2NP coated paperboard was transformed to a hydrophilic state by UVA irradiation, as was demonstrated earlier with cyclic wettability conversion by UVA and heat treatments [134, 135]. Both superhydrophobic and highly hydrophilic states after the UVA irradiation confirm that the TiO_2NPs remain on the surface even after calendering. The WCA values of TiO_2NP coated paperboard would have reached the level of the reference paperboard had all NPs been removed in the calendering nip. Therefore, the pressure caused by the nip compressed the NPs onto the paperboard surface reducing porosity and roughness that was followed by lowering and increasing of the WCA values for hydrophobic and hydrophilic surface, respectively.

4.1.2 Permanent planar fluidic channels

As discussed in the Materials and Methods, a typical issue with UVA activated wettability is reversibility, i.e. reversion to the initial superhydrophobicity of TiO_2NP coated paperboard within 60 days [136]. This would be a limiting factor as the shelf lifetime of such UVA activated products would be a significant disadvantage, leading to a product storage bottleneck. Therefore, in Paper III a procedure was developed to convert these functionalized channels permanently with a two-stage wetting procedure. The designed channel area is exposed to UVA light that converts it to hydrophilic. Then the channel is wetted, during which the LFS deposited TiO_2 nanoparticles are removed from the wetted area either to the edges or deeper into the pores of the base paperboard. The hydrophilic surface without first stage wetting can be returned to the initial superhydrophobic state by heat treatment in an oven. The schematics of the procedure

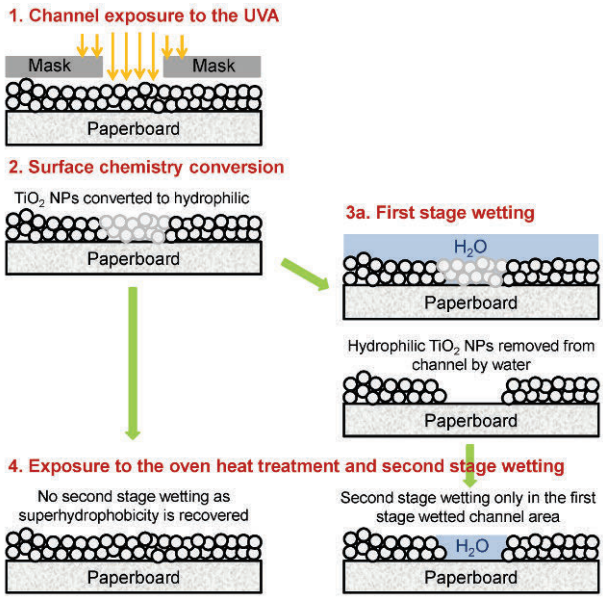

Figure 4.3: Formation of permanent channels on TiO_2 nanoparticle coated paperboard [Paper III]

are presented in Fig. 4.3.

Figure 4.4 shows an SEM image of the different areas. The area outside the UVA activation shows a typical pattern of LFS deposited TiO_2 nanoparticles having a highly porous structure with large surface area. The channel is clearly visible in Fig. 4.4b) as the first stage wetting effectively removed nanoparticles from the exposed channel area. Additionally, the pigment coating of the base paperboard is clearly visible in the channel area that is very similar the surface of the reference paperboard without NP coating. It can be concluded from the SEM images that the first stage wetting permanently removes the nanoparticles from the channel area. There is no coffee stain effect at the edges of the channel, i.e. no accumulation or aggregation of TiO_2NPs were observed.

To confirm the SEM results, a complementary study was carried out by using ToF-SIMS to measure the chemical properties of the UVA exposed area. Figure 4.5 summarizes the SEM and ToF-SIMS results of UVA exposed and oven treated samples from which the left side has been exposed to first stage wetting and the right hand side not. The difference is clear: no significant changes in the surface morphology or chemical map was observable without first stage wetting. This also supports the previous findings with switchable superhydrophobic surfaces [67, 134]. On the contrary, the channel area is clearly visible both in SEM and ToF-SIMS images after the first stage wetting. The correlation between the SEM and ToF-SIMS results agrees well with the used mask with a width of 1 mm for the channel exposure.

Finally, the mass/charge ratios of the secondary ions from the ToF-SIMS measurements are displayed in Fig. 4.6. Significant changes were observed in the spectra. For example, the peak at $m/z = 39.96$ corresponding to calcium was only observable in the first stage wetted sample. ToF-SIMS is a highly surface sensitive method with sample analyzing depth around 2 nm. In the non-wetted sample the whole sample surface is covered by the LFS deposited TiO_2NPs. Therefore, the ejected fragments originate from the LFS deposited NPs, whereas the first stage

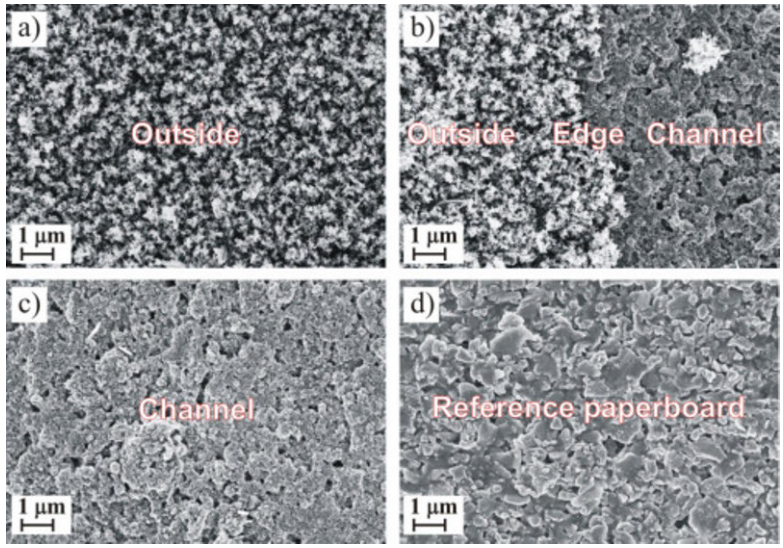

Figure 4.4: SEM images of the channel area [Paper III]

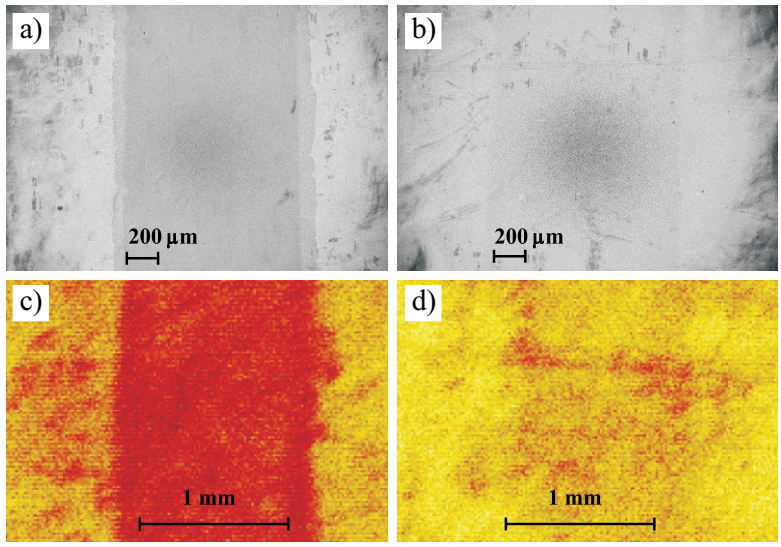

Figure 4.5: SEM images and ToF-SIMS mapping of the channel area with (a,c) and without (b,d) first stage wetting of the TiO_2NP coated paperboard [Paper III]

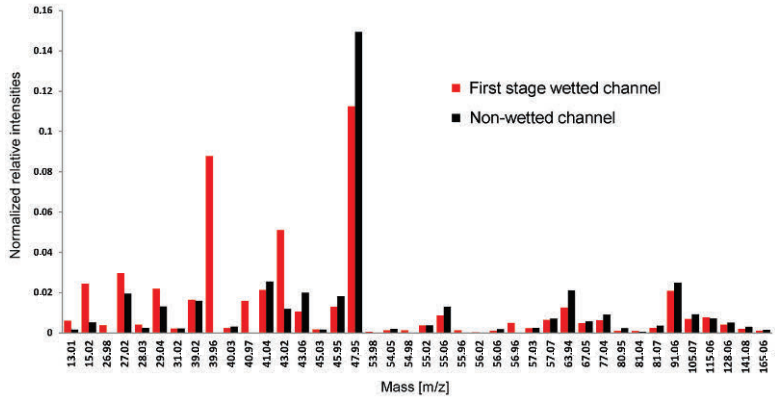

Figure 4.6: Tof-SIMS spectrum of the channel area [Paper III]

wetted sample displays the pigment coating of the base paperboard containing kaolin clay and calcium carbonate. Clearly, the calcium peak originated from these base paperboard pigment particles. Removal of TiO_2NPs is also supported by the reduction of Ti based peaks that are located at m/z = 45.95 (Ti), 47.95 (Ti), 63.94 (TiO), and 81.07 (TiO_2).

The results with first stage wetted samples show that the water exposed areas remain permanently in the hydrophilic state that resembles wettability of the used paperboard substrate, and the developed protocol avoids all issues related to reversible wetting conversion.

4.2 SERS on paper-based structures

SERS analysis, as it has typically been designed to date, has two common drawbacks: first, the used analytes typically stain the used substrate, and the SERS substrates can only be used once. Secondly, the SERS substrates are typically made on glass that prevents a roll-to-roll type manufacturing process, which could significantly reduce the cost of the SERS active substrates.

In this work two different approaches for making SERS active substrates were used in Papers II and IV. Paper II demonstrated the proof-of-concept type approach with LFS deposited Ag NPs on glass substrate that was expanded to paperboard substrate in Paper IV. Additionally, inkjet printing with AgNP ink was used in both papers as a well-established reference.

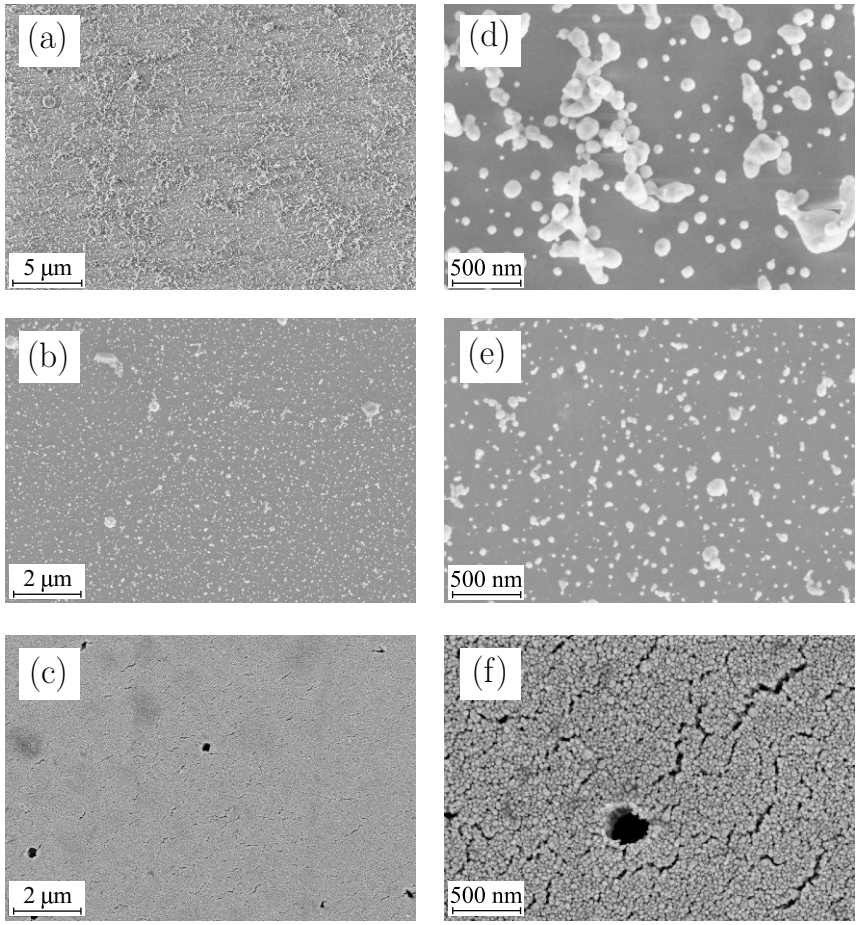

Figure 4.7: SEM images of silver nanoparticle deposited surfaces: (a) LFS 60 s 90 nm + 10×30 nm, (b) LFS 100×90 nm + 1×30 nm, (c) inkjet printed surface with DS 45 µm, and (d-f) the corresponding high magnification images. [Paper II]

Figure 4.7 shows low and high magnification images of LFS deposited (with two different deposition parameters) and inkjet printed AgNPs. In Fig. 4.7a) both indirect LFS deposition with a tube and direct deposition with a rotating carousel was used: first, a 60 s deposition time was used with flame for 90 nm average particle diameter followed by 10 passes through the flame for 30 nm particles (sample 60 s 90 nm + 10×30nm). The long deposition time induces aggregation of the deposited AgNPs into larger clusters as clearly seen in Fig. 4.7d). Figures 4.7b) and e) show the corresponding images for direct deposition in which 100 sweeps of the flame with 90 nm particle diameter were followed by a single sweep of the flame with 30 nm particle diameter (sample 100×90 nm + 1×30 nm). The sample surface was covered with smaller particles and less clustering was observed compared to the indirect deposition in Figs. 4.7a) and d). Finally, Figs. 4.7c) and f) show the inkjet printed AgNPs. A full coverage of the SEM image area is seen in both images as the images were captured from the center of the 10 pL printed dot. The typical diameter of the inkjet printed AgNPs was within 20 to 50 nm range in agreement with the specifications given by the ink manufacturer (Sun Chemicals, US).

Figure 4.8 presents the corresponding SERS spectra of crystal violet (CV) sample solution for the three different substrates with three different analyte concentrations from 10 nM to 1 µM. In all samples all concentrations displayed a typical fingerprint of CV molecules. Two different peaks were used for evaluating the sensitivity of the substrates: 1 586 cm^{-1} and 1 618 cm^{-1}. The sensitivity was calculated by comparing the peak signal intensity to the background intensity, i.e. a peak contrast was calculated. For the lowest 10 nM concentration the observed peak contrast values were 1.85, 1.16, and 1.57 at 1 586 cm^{-1} and 2.00, 1.29, and 2.33 for 1 618 cm^{-1}.

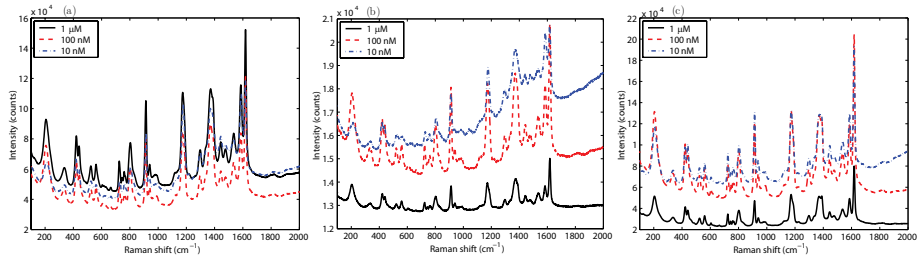

Figure 4.8: Measured SERS spectra of LFS deposited a) 60 s 90 nm + 10×30 nm and b) 100×90 nm + 1×30 nm AgNPs, and c) inkjet printed sample with DS 45 µm on glass substrate [Paper II]

Table 4.1: High resolution XPS data with relative carbon amounts (%), constituted in C-C, C-O and C=O configurations, respectively, at different curing temperatures [Paper II].

C	eV	C-C	SD	eV	C-O	SD	eV	C=O	SD
DS45 (120°C)	284.55	54.51	1.36	285.69	29.06	2.22	287.35	16.44	0.89
DS45 (200°C)	284.68	61.04	1.31	285.91	22.63	1.98	287.76	16.33	1.23
DS60 (120°C)	284.57	49.01	1.91	285.78	31.07	1.97	287.47	19.92	0.49
DS60 (200°C)	284.80	64.06	1.28	286.17	21.20	1.26	288.05	14.74	1.47
DS85 (120°C)	284.70	55.65	2.28	286.14	31.09	1.83	287.93	13.26	0.72
DS85 (200°C)	284.79	68.44	1.19	286.25	16.92	0.80	288.16	14.65	1.18

This indicates that both the LFS sample with long deposition time and the inkjet printed sample were suitable for detecting down to 10 nM CV concentration whereas for the LFS sample with direct deposition 100 nM CV concentration was required for a peak contrast of 1.37 and 1.86, respectively.

Thermal curing was needed to guarantee ink setting on the used glass substrate. Two different curing temperatures were utilized at 120°C and 200°C, and the samples were kept in an oven for 30 min for both temperatures. It was unexpected that the higher curing temperature of 200°C completely removed the SERS activity. An XPS study was carried out to study the observed surface passivation. The high resolution XPS data for carbon is in Table 4.1.

From Table 4.1 it can be concluded that the higher curing temperature significantly changed the C-O and C-C relative amounts. Higher curing temperature increased C-C amount whereas C-O amount was reduced. Ethylene glycol (EG) is typically used as a component in the ink formulations for inkjet printing. The boiling point of EG is 197.8°C. The observed changes in the XPS relative carbon amounts can be linked to the EG boiling, i.e. the EG component was boiled and burned away from the inkjet solutions at the higher curing temperature. This can lead to a carbonaceous covering of the AgNPs. It is well-known that the SERS signal is extremely surface sensitive with signal decaying to r^{-10} for spherical particles [84]. Therefore, even a thin layer on top of the AgNPs can passivate the SERS signal generation as the analytes can not reach the silver surface with the highest local electric field.

Paperboard functionalized with AgNPs would be a cost-effective alternative for traditional glass substrates. Combination with roll-to-roll production flow would provide large-scale production. However, the inherent luminescence both from cellulose fibres and from pigment coating components can overcrowd the rather weak Raman signal.

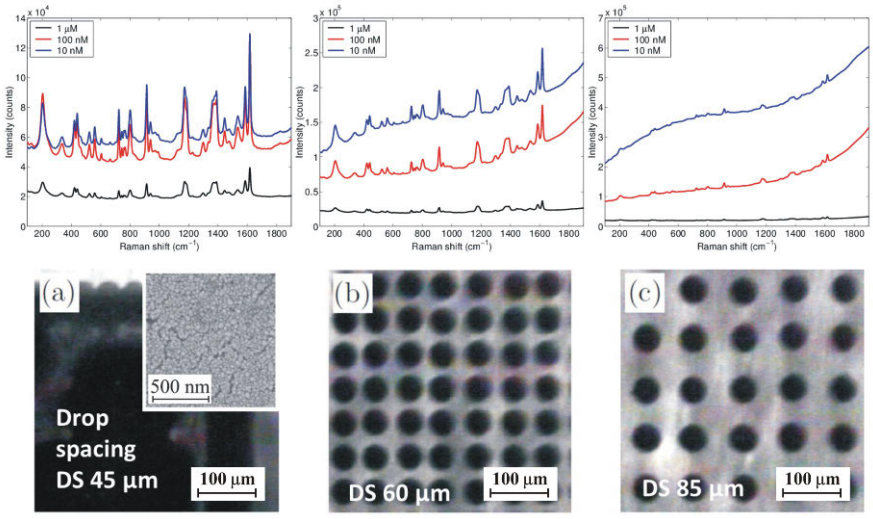

Figure 4.9: Measured Raman intensities and SEM images of inkjet printed AgNPs on paperboard. The dotted line shows the used laser spot size for the Raman signal excitation. [Paper IV]

As a starting point in Paper IV, inkjet printing with controlled surface coverage was studied. The surface coverage can easily be controlled simply by changing the drop spacing on the sample surface. Figure 4.9 shows the measured Raman intensities with corresponding low magnification SEM images printed with varied drop spacing (DS) values. With 45 µm spacing, the paperboard surface was fully covered by silver nanoparticles whereas 85 µm spacing resulted in less than 50% coverage exposing the base paperboard for a laser light excitation.

Typical CV Raman peaks are clearly visible in Fig. 4.9a) with 45 µm DS value. The number of counts is an order of magnitude larger for DS value 60 µm, and an additional order of magnitude was observed for DS value 85 µm. This highlights the importance of luminescence: the laser light used for the Raman signal generation also excited the base paper for 60 and 85 µm spacing. For 45 µm spacing the full coverage completely blocks the luminescence generation and thus allow reliable detection of the Raman signal. In Fig. 4.9c), the Raman peaks are almost indistinguishable from the elevated background due to the strong luminescence.

There are several ways to solve the problem with inherent luminescence. It is well-known in literature [214, 215] that Raman signal has lifetime less than a picosecond that is in contrary to luminescence with signal lifetime in thousands of picoseconds. Nowadays commercial time-gated Raman spectrometers are available [216]. However, for simple point-of-care type diagnostic applications such sophisticated time-gated instruments may be challenging and too expensive. Hence, it would be beneficial to have a cost-efficient, disposable SERS active substrates suitable for a typical SERS measurement.

In Paper IV a cost-efficient printable graphite coating was developed that can block the background luminescence. The approach here was the same as presented in Fig. 4.9a) but the expensive silver was replaced by simple carbon coating. A flexography test printer was used with carbon ink to print the luminescence suppressive layer as presented in Fig. 4.10. Several successive prints were examined that increased print density and the carbon coating thickness.

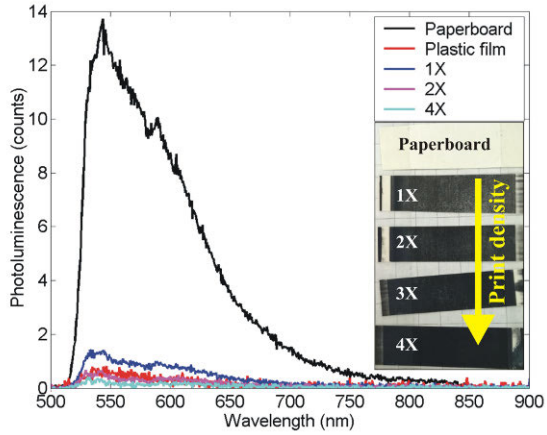

Figure 4.10: Measured luminescence (excitation at 490 nm) from flexographic printed carbon coated paperboards with successive prints compared to a PET plastic film. [Paper IV]

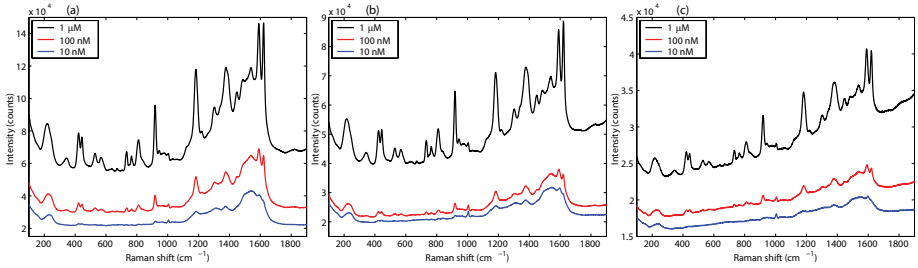

Figure 4.11: Raman intensities of LFS deposited AgNPs with a) 50×90 nm + 10×50 nm, b) 25×90 nm + 10×50 nm, and c) a) 10×90 nm + 10×50 nm with three different CV analyte concentrations [Paper IV]

It was observed that even a single print reduced the luminescence by an order of magnitude, and two prints were able to reduce the luminescence almost completely. It is noteworthy that the used anilox roll was not optimized for the used ink, and it is presumable that with an optimized design even a single print can suppress the luminescence sufficiently for practical applications.

The carbon coated paperboards were functionalized with direct LFS deposited AgNPs with three different amounts: first, 10 sweeps with 90 nm particles followed by 10 sweeps of 50 nm particles, secondly 25 sweeps with 90 nm particles followed by 10 sweeps of 50 nm particles, and finally, 50 sweeps with 90 nm particles followed by 10 sweeps of 50 nm particles. The corresponding Raman spectra are presented in Fig. 4.11. Comparing the measured spectra between the glass presented in Fig. 4.8 and carbon coated paperboard surface presented in Fig. 4.11, the carbon G-band around 1 582 cm^{-1} can be observed in the carbon coated paperboard case. This is especially visible at low CV concentrations, with the negative result that the CV peak contrast at 1 618 cm^{-1} is significantly reduced. Therefore, two additional peaks were analyzed outside the carbon Raman G-band.

A typical spectral fingerprint of CV was clearly observed for all the samples. However, the sensitivity of the paperboard structures was lower compared to the glass substrates [Paper II]. The Raman peak contrast to background was analyzed at three locations: 445, 918, and 1 618 cm^{-1}. The highest peak contrast values were observed for peak at 918 cm^{-1}. For comparison to glass substrates, the observed peak contrast values for 1 µM CV solution at 1 618 cm^{-1} were 1.31 (50×90 nm + 10×50 nm) and 1.30 (50×90 nm + 10×50 nm). These values show that the sensitivity of LFS deposited AgNPs on carbon coated paperboard is approximately two orders of magnitude lower than for glass substrates. However, it is worth emphasizing that without the carbon coating no Raman signal would be observable from paperboard.

4.3 Roll-to-roll coated and printed oxygen indicators for MAPs

Oxygen indicators were developed in Paper V. Methylene blue (MB) is a well-known heterocyclic aromatic compound that has a distinctive blue colour in the oxidized form that can be

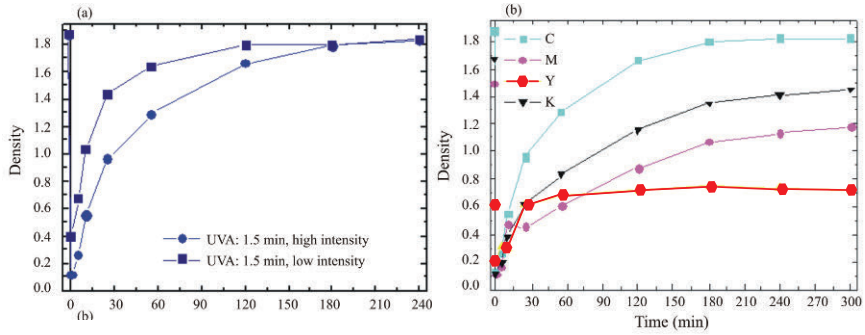

Figure 4.12: Dynamics of a) the cyan (C) density of RG coated indicator film under two different UVA intensities, and b) the cyan (C), magenta (M), yellow (Y) and black ('Karbon' K) components under high UVA intensity. [Paper V]

converted by reduction to the transparent leucomethylene blue form [210]. MB based functional inks can be printed or coated on paperboard or plastic for use as simple, cost-effective indicators, for example, in modified atmosphere packages.

Two different approaches were utilized. First, reverse gravure (RG) coating of MB-TiO_2NP ink on plastic film resulted in a uniform coating that can be patterned using a photomask with an UVA source. Alternatively, flexographic printing can be used with a pre-designed pattern to print the designed label that allows for a significant reduction of the used ink amount.

Both RG coated and flexographically printed labels are bleached by UVA exposure before sealing into oxygen free atmosphere. Subsequent exposure to oxygen is observed by the contrast increase, which converts reduced LMB into the oxidized MB form. Figure 4.12a) shows the dynamics of the cyan (C) component development in the indicator ink under two different UVA intensities. The dynamics of the oxidized form recovery can be adjusted by the used UVA intensity. The dynamics of the cyan (C), magenta (M), yellow (Y) and black (K) components under high intensity UVA illumination are presented in Fig. 4.12b) clearly show that cyan induced the largest contrast between the bleached and oxidized state.

In the flexographically printed labels the printed label becomes visible whereas, the RG coated and UVA patterned labels lose their contrast as the UVA bleached parts revert to the original density of the blue background. With anti-counterfeiting there is one clear benefit with the RG coated and UVA patterned labels: the exposed flexographically printed labels can be bleached by an external UVA source whereas the original pattern of the RG coated labels would lose the pattern as the whole surface would be bleached to transparent. The only way to regain the initial pattern would be to use a similar photomask as during the initial patterning.

Figure 4.13 shows several different photomask designs that have been used for UVA patterning of the RG coated plastic film. Both traditional 1D barcodes and 2D QR codes presented in Fig. 4.13a) can be masked on the coated functional ink. In addition, UVA patterning allows various designs: as an example, a fish package design with a warning text was tested both in positive and negative layouts, as shown in Fig. 4.13b). The exposure to air resulted in contrast loss of the UVA patterned designs within a few hours of exposure due to oxidation.

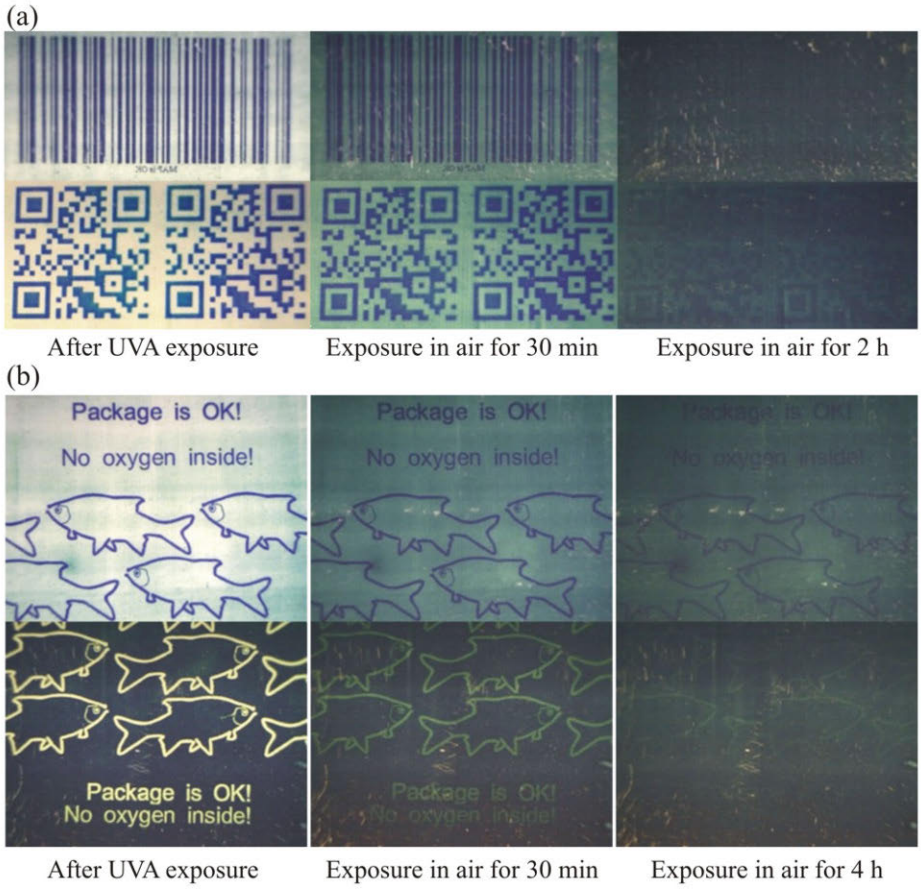

Figure 4.13: Reverse gravure coated and UVA patterned a) 1D barcodes and 2D QR codes and b) safety labels on plastic film after exposure to air [Paper V]

Such response time is sufficient for the designed applications, e.g. as oxygen indicators for the modified atmosphere packages. A similar approach has also been suggested for visible light using a riboflavin-ethylenediaminetetraacetic acid (EDTA) based solutions [217, 218].

The flexographically printed labels are presented in Fig. 4.14. Ink setting in flexography was tested for several different substrates ranging from commercial plastic film to multilayer coated paper [155] designed for printed electronics. A significant improvement can be achieved in print quality by controlling the porosity of the top coating that allows a quick and controlled ink setting. Additionally, paper provides a white background for high print contrast compared to transparent plastic films.

Figure 4.14 has a clear contrast for the MB-TiO_2 ink before exposure to UVA light that almost completely bleaches the printed pattern. A partial remaining contrast may be induced by the surface porosity as the UVA source may not reach the TiO_2NPs that have penetrated deeper in

Figure 4.14: Flexographically printed labels on paperboard after exposure to air [Paper V]

the pores. This issue can probably be solved by fine tuning of the pore size distribution and the used anilox rolls for the flexographic printing to optimize the ink setting on the sample surface. The initial contrast values are obtained after 2.5 h exposure to air.

As a summary, both RG coated and flexographic printed UVA activated labels can be used as oxygen indicators for modified atmosphere packages. Flexography uses significantly less functional ink but the RG coated structures have a clear benefit in applications with strong demand for anti-counterfeiting.

Chapter 5

Summary

This thesis deals with nanophotonic constructs on natural fibre based substrates with three main applications: controlled wettability, surface-enhanced Raman scattering (SERS) active substrates, and printed and coated oxygen sensors for modified atmosphere packages.

Controlled wettability plays a significant role in various industries ranging from paints and printing to non-wetting surfaces and microfluidics. Liquid flame spray (LFS) deposition of TiO_2 nanoparticles has been used for the past ten years to create a superhydrophobic surface on paperboard. The photocatalytic activity of TiO_2 under UVA light can be used to convert the initially superhydrophobic surface into a highly hydrophilic one, and the initial superhydrophobic state can be retrieved by heat treatment in an oven. A problem with TiO_2 UVA activated wettability is reversion: the surface loses the wetting properties without further activation by the UVA light within 60 days. A solution for this issue was developed using a first-stage wetting immediately after the UVA exposure that removes the converted, hydrophilic TiO_2 nanoparticles from the exposed areas. Hence, the designed exposed area can be converted to a permanently hydrophilic state. Additionally, durability of the LFS deposited nanoparticles was examined under compression in calendering, and it was observed that compression suppresses the high porosity of the deposited nanoparticle layer. However, the changes in wettability confirmed that the LFS deposited nanoparticles were not completely removed by compression. One possible application for these results is permanent planar fluidic channels that can be used, for example, in point-of-care (POC) diagnostic applications.

Silver nanoparticles have been used for decades to enhance inherently weak Raman scattering. The free electrons in metal nanoparticles are coupled with the incident light by plasmonic coupling inducing strong local electric fields in the vicinity of the nanoparticle surface. These local near-fields can be used to enhance a Raman signal (SERS) by several orders of magnitude via electromagnetic enhancement. The near-fields decay rapidly, and the analyte molecules need to be on the surface of metal nanostructures for high enhancement factors. Typically SERS active structures are manufactured on glass substrates. However, these structures can only be used for a single Raman measurement as the sample typically stains the used substrate. Therefore, it would be beneficial to have SERS active substrates that are cost-effective and can easily be discarded.

SERS active substrates were developed on paperboard using a simple flexographic carbon coating combined with LFS deposited silver nanoparticles. It was demonstrated that LFS is a suit-

able tool for silver nanoparticle deposition for SERS active structures on glass. However, on paperboard the luminescence from the background substrate is a problem as the SERS signal is lost in the stronger luminescence background. Two ways to overcome this problem were proposed: first, one can use inkjet printing with commercial silver ink to block the background luminescence. Unfortunately, a full silver coverage of the substrate surface was required that would be expensive. A better way to reduce luminescence is to use a simple carbon coating that can be printed by flexography. On top of the carbon coating even individual silver nanoparticles deposited by the LFS can be used to excite and enhance SERS. This allowed a significant reduction of the used silver amount.

Finally, commercial TiO_2 nanoparticles were applied together with methylene blue dye as an oxygen indicator ink. Methylene blue has a distinct blue color in an oxidized form that can be converted to the transparent leucomethylene blue form by UVA light excitation. Two different approaches were utilized: reverse gravure coated films and flexographically printed labels. Both structures were UVA bleached before sealing into an oxygen free environment. The reverse gravure printed films can be patterned by UVA light with a photomask, which design one can change freely. For example, 1D barcodes and 2D QR codes were demonstrated that change color upon exposure to oxygen resulting in a lost contrast of the patterned image. The developed simple indicator structures can be used as oxygen sensors, for example, in modified atmosphere packages.

One example, in which renewable sensors are expected to be of key importance, is the internet of things (IoT), seen today as a rapidly emerging field. A prerequisite for IoT to happen on a global scale is it must be cost-effective, presumably roll-to-roll processable for efficient manufacture, incorporating smart structures and sensors that can be integrated, say, into packages. For this development to be sustainable, there is a great demand for green and biodegradable electronics. There is a large potential for significant cost-savings, for example, with smart refrigerators combined with integrated biosensors in packages. Currently, in the western countries approximately 100 kg of food/capita is lost annually [201], whereas famine is a problem in other parts of the world. Better control of food shelf-life, and longevity in storage, could, therefore, contribute enormously to relieving waste.

Such applications highlight the potential for the forest industry to contribute to the improved sustainable life quality for future. There are already now in the market the first examples of printed intelligence, such as the Stora Enso developed package with an RFID circuitry for monitoring medical drug dosage regimes for elderly people. Additionally, POC analytics can provide better access for diagnostics in developing countries. One possibility could be the combination of recyclable POC sensors with smart phones. Such quick remote health care could offer large potential for cost savings with quick diagnostics, for example preventing unnecessary antibiotic use for virus infections. Remote health monitoring could also have significant epidemiologic implications, for example, in monitoring of influenza, ebola, or current corona outbreak.

These examples above reflect a larger change taking place in human society. Futurological studies [219] have indicated that the world is now entering into the sixth long wave of innovation that is driven by a twin need: new innovations need to improve productivity similar to the previous waves but also reduce the environmental burden at the same time. The need for sustainable solutions becomes evident by, for example, the sixth rapid extinction wave of species and loss of biodiversity, lack of both renewable and non-renewable raw materials, and climate change. Planetary boundaries, which set the limit for Earth ecosystems functioning unaltered, are start-

ing to become reached or already exceeded in some areas according to a recent report [220]. Exceeding planetary boundaries can result in dramatic, unfavorable changes in the environment. Therefore, the demand for sustainability is changing business models throughout industries.

Contributing to the need for a new wave of sustainable innovation, this work also needed to address certain problems arising in the design of functional surfaces. This was exemplified by two cases. In the first case, controlled wettability was achieved using a photocatalytic wettability conversion of initially hydrophobic TiO_2NPs, and the wettability conversion was converted to permanent by the developed first stage wetting protocol. In the second case, AgNPs were deposited on glass and paperboard for SERS activity. However, the problem of luminescence from the base paperboard is a strong handicap for Raman analysis that is orders of magnitude weaker in strength. This problem was solved by a full coverage of the paperboard surface by either silver or graphite carbon coating that prevented the excitation of the luminescence from the base paperboard. It was observed that Raman signal level from carbon coated paperboard substrates was weaker compared to glass substrate. For improved SERS results on paperboard it would be beneficial to have simultaneous characterization of surface morphology and local Raman activity that could be achieved, for example, by using TERS analysis. Unfortunately, no access to such detailed characterization was available during this thesis work.

For future work, understanding the local photonic response would yield detailed insight about the generation of Raman hot spots, which dominate the measured SERS spectra. This information can be used to optimize the LFS process parameters for improved SERS activity on paperboard and glass substrates.

Natural fibre based substrates are expected to have an increasing importance in the future as the demands for sustainability are growing in all industrial sectors. Cellulose is abundant, renewable, recyclable, and widely available raw material. With new functionalities the forest products industry can move up the value chain ladder, promoting both economically and ecologically sustainable development. I believe that developments in the field of functional materials applied to cellulose compounds, networks and substrates can place the forest products sector in a position to meet the future demands of the rapidly changing world.

References

[1] R. P. Feynman, "There's plenty of room at the bottom," *Eng. Sci.* **23**, 22–36 (1960).

[2] M. Pantsar and K. Herlevi *et al.*, *Leading the cycle – Finnish Road Map to a Circular Economy 2016–2025* (Sitra, Helsinki, 2016).

[3] Masson-Delmotte, V. *et al.* Working Group III Contribution, *Global warming of 1.5°C. An IPCC Special Report on the impacts of global warming of 1.5°C above pre-industrial levels and related global greenhouse gas emission pathways, in the context of strengthening the global response to the threat of climate change, sustainable development, and efforts to eradicate poverty* (IPCC SR15 Full Report, New York, 2018).

[4] O. R. Edenhofer *et al.* Working Group III Contribution, *Climate Change 2014 – Mitigation of Climate Change* (IPCC, New York, 2014).

[5] T. A. Boden, G. Marland, and R. J. Andres, "Global, regional, and national fossil-fuel CO_2 emissions," *Carbon Dioxide Information Analysis Center* USA (2017).

[6] J. S. Pal and E. A. B. Eltahir, "Future temperature in southwest Asia projected to exceed a threshold for human adaptability," *Nat. Clim. Change* **6**, 197–200 (2016).

[7] S. Kang and E. A. Eltahir, "North China plain threatened by deadly heatwaves due to climate change and irrigation," *Nat. Commun.* **9**, 2894 (2018).

[8] G. Kopp and J. L. Lean, "A new, lower value of total solar irradiance: Evidence and climate significance," *Geophys. Res. Lett.* **38**, L01706 (2011).

[9] National Renewable Laboratory, *Best research cell efficiencies* (NREL, 2020).

[10] B. O'Regan and M. Grätzel, "A low-cost, high-efficiency solar cell based on dye-sensitized colloidal TiO_2 films," *Nature* **353**, 737–740 (1991).

[11] B. E. Hardin, H. J. Snaith, and M. D. McGehee, "The renaissance of dye-sensitized solar cells," *Nat. Photonics* **6**, 162–169 (2012).

[12] A. Fujishima, K.-I. Honda, and S.-I. Kikuchi, "Photosensitized electrolytic oxidation on semiconducting n-type TiO_2 electrode," *J. Soc. Chem. Ind.* **72**, 108–113 (1969).

[13] A. Fujishima and K. Honda, "Electrochemical photolysis of water at a semiconductor electrode," *Nature* **238**, 37–38 (1972).

[14] J. Schneider, M. Matsuoka, M. Takeuchi, J. Zhang, Y. Horiuchi, M. Anpo, and D. W. Bahnemann, "Understanding TiO_2 photocatalysis: Mechanisms and materials," *Chem. Rev.* **114**, 9919–9986 (2014).

[15] National Renewable Laboratory, *https://www.nrel.gov/grid/solar-resource/spectra-am1.5.html* (NREL, 2014).

[16] C. Dette, M. A. Perez-Osorio, C. S. Kley, P. Punke, C. E. Patrick, P. Jacobson, F. Giustino, S. J. Jung, and K. Kern, "TiO_2 anatase with a bandgap in the visible region," *Nano Lett.* **14**, 6533–6538 (2014).

[17] H. Song, C. Li, Z. Lou, Z. Ye, and L. Zhu, "Effective formation of oxygen vacancies in black TiO_2 nanostructures with efficient solar-driven water splitting," *ACS Sustain. Chem. Eng.* **5**, 8982–8987 (2017).

[18] M. F. Cardinal, E. Vander Ende, R. A. Hackler, M. O. McAnally, P. C. Stair, G. C. Schatz, and R. P. Van Duyne, "Expanding applications of SERS through versatile nanomaterials engineering," *Chem. Soc. Rev.* **46**, 3886–3903 (2017).

[19] C. Clavero, "Plasmon-induced hot-electron generation at nanoparticle/metal-oxide interfaces for photovoltaic and photocatalytic devices," *Nat. Photonics* **8**, 95–103 (2014).

[20] S. Tan, A. Argondizzo, J. Ren, L. Liu, J. Zhao, and H. Petek, "Plasmonic coupling at a metal/semiconductor interface," *Nat. Photonics* **11**, 806–812 (2016).

[21] J. S. DuChene, G. Tagliabue, A. J. Welch, W.-H. Cheng, and H. A. Atwater, "Hot hole collection and photoelectrochemical CO_2 reduction with plasmonic Au/p-GaN photocathodes," *Nano Lett.* **18**, 2545–2550 (2018).

[22] U. Aslam, S. Chavez, and S. Linic, "Controlling energy flow in multimetallic nanostructures for plasmonic catalysis," *Nat. Nanotechnol.* **12**, 1000–1005 (2017).

[23] P. Christopher, H. Xin, and S. Linic, "Singular characteristics and unique chemical bond activation mechanisms of photocatalytic reactions on plasmonic nanostructures," *Nat. Mater.* **11**, 1044–1050 (2012).

[24] E. Kazuma, J. Jung, H. Ueba, M. Trenary, and Y. Kim, "Real-space and real-time observation of a plasmon-induced chemical reaction of a single molecule," *Science* **360**, 521–526 (2018).

[25] K. J. Klabunde, J. Stark, O. Koper, C. Mohs, D. G. Park, S. Decker, Y. Jiang, I. Lagadic, and D. Zhang, "Nanocrystals as stoichiometric reagents with unique surface chemistry," *J. Phys. Chem.* **100**, 12142–12153 (1996).

[26] P. Buffat and J.-P. Borel, "Size effect on the melting temperature of gold particles," *Phys. Rev. A* **13**, 2287–2298 (1976).

[27] J. Zhang, J.-Y. Ou, N. Papasimakis, Y. Chen, K. F. MacDonald, and N. I. Zheludev, "Continuous metal plasmonic frequency selective surfaces," *Opt. Express* **19**, 23279–23285 (2011).

[28] C. A. Mirkin, "The beginning of a small revolution," *Small* **1**, 14–16 (2005).

[29] D. Gall, "Electron mean free path in elemental metals," *J. Appl. Phys.* **119**, 085101 (2016).

[30] T. Groves, "Electron beam lithography," in *Nanolithography*, M. Feldman, ed. (Woodhead Publishing, 2014), pp. 80–115.

[31] A. Dufresne, "Nanocellulose: A new ageless bionanomaterial," *Mater. Today* **16**, 220–227 (2013).

[32] B. Bhushan, *Biomimetics–Bioinspired Hierarchical-Structured Surfaces for Green Science and Technology*, 3rd ed. (Springer, 2018).

[33] H. J. Ensikat, P. Ditsche-Kuru, C. Neinhuis, and W. Barthlott, "Superhydrophobicity in perfection: The outstanding properties of the lotus leaf," *Beilstein J. Nanotech.* **2**, 152–161 (2011).

[34] S. Vignolini, P. J. Rudall, A. V. Rowland, A. Reed, E. Moyroud, R. B. Faden, J. J. Baumberg, B. J. Glover, and U. Steiner, "Pointillist structural color in Pollia fruit," *Proc. Nat. Acad. Sci.* **109**, 15712–15715 (2012).

[35] P. Vukusic, B. Hallam, and J. Noyes, "Brilliant whiteness in ultrathin beetle scales," *Science* **315**, 348 (2007).

[36] S. Zylinski and S. Johnsen, "Mesopelagic cephalopods switch between transparency and pigmentation to optimize camouflage in the deep," *Curr. Biol.* **21**, 1937–1941 (2011).

[37] G. L. Messing, S.-C. Zhang, and G. V. Jayanthi, "Ceramic powder synthesis by spray pyrolysis," *J. Am. Ceram. Soc.* **76**, 2707–2726 (1993).

[38] K. Okuyama and I. Wuled Lenggoro, "Preparation of nanoparticles via spray route," *Chemi. Engin. Sci.* **58**, 537–547 (2003).

[39] P. S. Patil, "Versatility of chemical spray pyrolysis technique," *Mater. Chem. Phys.* **59**, 185–198 (1999).

[40] J. Leng, Z. Wang, J. Wang, H.-H. Wu, G. Yan, X. Li, H. Guo, Y. Liu, Q. Zhang, and Z. Guo, "Advances in nanostructures fabricated via spray pyrolysis and their applications in energy storage and conversion," *Chem. Soc. Rev.* **48**, 3015–3072 (2019).

[41] G. D. Ulrich, "Theory of particle formation and growth in oxide synthesis flames," *Combust. Sci. Technol.* **4**, 47–57 (1971).

[42] S. E. Pratsinis, "Flame aerosol synthesis of ceramic powders," *Prog. Energ. Combust. Sci.* **24**, 197–219 (1998).

[43] W. Y. Teoh, R. Amal, and L. Mädler, "Flame spray pyrolysis: An enabling technology for nanoparticles design and fabrication," *Nanoscale* **2**, 1324–1347 (2010).

[44] S. Thybo, S. Jensen, J. Johansen, T. Johannessen, O. Hansen, and U. J. Quaade, "Flame spray deposition of porous catalysts on surfaces and in microsystems," *J. Catal.* **223**, 271–277 (2004).

[45] P. Moravec, J. Smolik, and V. V. Levdansky, "Preparation of TiO_2 fine particles by thermal decomposition of titanium tetraisopropoxide vapor," *J. Mater. Sci. Lett.* **20**, 2033–2037 (2001).

[46] T. Pluym, Q. Powell, A. Gurav, T. Ward, T. Kodas, L. Wang, and H. Glicksman, "Solid silver particle production by spray pyrolysis," *J. Aerosol Sci.* **24**, 383–392 (1993).

[47] S. Stopic, P. Dvorak, and B. Friedrich, "Synthesis of spherical nanosized silver powder by ultrasonic spray pyrolysis," *Metall* **60**, 377–382 (2006).

[48] A. Pitkänen, J. M. Mäkelä, M. Nurminen, A. Oksanen, K. Janka, H. K. J. Keskinen and, J. K. Liimatainen, S. Hellsten, and T. Määttä, "Numerical Study of silica particle formation in turbulent H_2/O_2 flame," *IFRF Combust. J.* **34**, 200509 (2005).

[49] R. Mueller, H. K. Kammler, K. Wegner, and S. E. Pratsinis, "OH surface density of SiO_2 and TiO_2 by thermogravimetric analysis," *Langmuir* **19**, 160–165 (2003).

[50] K. J. Brobbey, J. Haapanen, M. Gunell, M. Toivakka, J. M. Mäkelä, E. Eerola, R. Ali, M. R. Saleem, S. Honkanen, J. Bobacka, and J. J. Saarinen, "Controlled time release and leaching of silver nanoparticles using a thin immobilizing layer of aluminum oxide," *Thin Solid Films* **645**, 166–172 (2018).

[51] H. Keskinen, J. Mäkelä, M. Vippola, M. Nurminen, J. Liimatainen, T. Lepistö, and J. Keskinen, "Generation of silver/palladium nanoparticles by liquid flame spray," *J. Mater. Res.* **19**, 1544–1550 (2004).

[52] H. Keskinen, J. M. Mäkelä, M. Aromaa, J. Keskinen, S. Areva, C. V. Teixeira, J. B. Rosenholm, V. Pore, M. Ritala, M. Leskelä, M. Raulio, M. S. Salkinoja-Salonen, E. Levänen, and T. Mäntylä, "Titania and titania-silver nanoparticle deposits made by liquid flame spray and their functionality as photocatalyst for organic- and biofilm removal," *Catal. Lett.* **111**, 127–132 (2006).

[53] J. Haapanen, M. Aromaa, H. Teisala, M. Tuominen, M. Stepien, J. Saarinen, M. Heikkilä, M. Toivakka, J. Kuusipalo, and J. Mäkelä, "Binary TiO_2/SiO_2 nanoparticle coating for controlling the wetting properties of paperboard," *Mater. Chem. Phys.* **149–150**, 230–237 (2015).

[54] M. Rajala, K. Janka, and P. Kykkänen, "An industrial method for nanoparticle synthesis with a wide range of compositions," *Rev. Adv. Mater. Sci.* **5**, 493–497 (2003).

[55] K. J. Brobbey, J. Haapanen, M. Gunell, J. M. Mäkelä, E. Eerola, M. Toivakka, and J. J. Saarinen, "One-step flame synthesis of silver nanoparticles for roll-to-roll production of antibacterial paper," *Appl. Surf. Sci.* **420**, 558–565 (2017).

[56] J. M. Mäkelä, M. Aromaa, H. Teisala, M. Tuominen, M. Stepien, J. J. Saarinen, M. Toivakka, and J. Kusipalo, "Nanoparticle deposition from liquid flame spray onto moving roll-to-roll paperboard material," *Aerosol Sci. Technol.* **45**, 817–827 (2011).

[57] M. Stepien, *Physico-Chemical Characterization of Nanoparticle Coated Paper*, PhD thesis (Åbo Akademi University, 2014).

[58] L. Mädler, A. Roessler, S. Pratsinis, T. Sahm, A. Gurlo, N. Barsan, and U. Weimar, "Direct formation of highly porous gas-sensing films by in situ thermophoretic deposition of flame-made Pt/SnO_2 nanoparticles," *Sens. Actuat. B Chem.* **114**, 283–295 (2006).

[59] P. Kulkarni and P. Biswas, "A Brownian dynamics simulation to predict morphology of nanoparticle deposits in the presence of interparticle interactions," *Aerosol Sci. Technol.* **38**, 541–554 (2004).

[60] K. J. Brobbey, J. Haapanen, J. M. Mäkelä, M. Gunell, E. Eerola, E. Rosqvist, J. Peltonen, J. J. Saarinen, and M. Toivakka, "Characterization of flame coated nanoparticle surfaces with antibacterial properties and the heat-induced embedding in thermoplastic-coated paper," *SN Appl. Sci.* **1**, 65 (201).

[61] K. J. Brobbey, J. Haapanen, J. M. Mäkelä, M. Gunell, E. Eerola, E. Rosqvist, J. Peltonen, J. J. Saarinen, M. Tuominen, and M. Toivakka, "Effect of plasma coating on antibacterial activity of silver nanoparticles," *Thin Solid Films* **672**, 75–82 (2019).

[62] A. Tricoli, A. S. Wallerand, and M. Righettoni, "Highly porous TiO_2 films for dye sensitized solar cells," *J. Mater. Chem.* **22**, 14254–14261 (2012).

[63] T. Rudin, K. Tsougeni, E. Gogolides, and S. E. Pratsinis, "Flame aerosol deposition of TiO_2 nanoparticle films on polymers and polymeric microfluidic devices for on-chip phosphopeptide enrichment," *Microelectron. Eng.* **97**, 341–344 (2012).

[64] A. Tricoli, M. Graf, F. Mayer, S. Kuühne, A. Hierlemann, and S. E. Pratsinis, "Micropatterning layers by flame aerosol deposition-annealing," *Adv. Mater.* **20**, 3005–3010 (2008).

[65] K. Gross, J. Tikkanen, J. Keskinen, V. Pitkänen, M. Eerola, R. Siikamäki, and M. Rajala, "Liquid flame spraying for glass coloring," *J. Therm. Spray Technol.* **8**, 583–589 (1999).

[66] H. Teisala, M. Tuominen, M. Aromaa, J. M. Mäkelä, M. Stepien, J. J. Saarinen, M. Toivakka, and J. Kuusipalo, "Development of superhydrophobic coating on paperboard surface using the liquid flame spray," *Surf. Coat. Technol.* **205**, 436–445 (2010).

[67] M. Stepien, J. J. Saarinen, H. Teisala, M. Tuominen, M. Aromaa, J. Kuusipalo, J. M. Mäkelä, and M. Toivakka, "Surface chemical characterization of nanoparticle coated paperboard," *Appl. Surf. Sci.* **258**, 3119–3125 (2012).

[68] D. Valtakari, R. Bollström, M. Tuominen, H. Teisala, M. Aromaa, M. Toivakka, J. Kuusipalo, J. M. Mäkelä, and J. J. S. Jun Uozumi4, "Flexographic printing of PEDOT:PSS on coated papers for printed functionality," *J. Print. Media Technol. Res.* **2**, 7–13 (2013).

[69] J. M. Mäkelä, J. Haapanen, J. Harra, P. Juuti, and S. Kujanpää, "Liquid flame spray — A hydrogen-oxygen flame based method for nanoparticle synthesis and functional nanocoatings," *KONA Powder Part. J.* **34**, 141–154 (2017).

[70] M. Nogi, S. Iwamoto, A. N. Nakagaito, and H. Yano, "Optically transparent nanofiber paper," *Adv. Mater.* **21**, 1595–1598 (2009).

[71] Z. Fang, H. Zhu, Y. Yuan, D. Ha, S. Zhu, C. Preston, Q. Chen, Y. Li, X. Han, S. Lee, G. Chen, T. Li, J. Munday, J. Huang, and L. Hu, "Novel nanostructured paper with ultrahigh transparency and ultrahigh haze for solar cells," *Nano Lett.* **14**, 765–773 (2014).

[72] M. A. Hubbe, J. J. Pawlak, and A. A. Koukoulas, "Paper's appearance: A review," *Bioresources* **3**, 627–665 (2008).

[73] E. M. Purcell and C. R. Pennypacker, "Scattering and absorption of light by nonspherical dielectric grains," *Astrophys. J* **186**, 705–714 (1973).

[74] A. Penttilä, K. Lumme, and L. Kuutti, "Light-scattering efficiency of starch acetate pigments as a function of size and packing density," *Appl. Opt.* **45**, 3501–3509 (2006).

[75] G. Mie, "Beitrage zur optik truber median, speziell kolloidaler metallosungen," *Ann. der Physik (Leipzig)* **25**, 377–445 (1908).

[76] C. V. Raman and K. S. Krishnan, "A new type of secondary radiation," *Nature* **121**, 501–502 (1928).

[77] K. Kneipp, M. Moskovits, and H. Kneipp, *Surface-Enhanced Raman Scattering* (Springer, Heidelberg, 2006).

[78] M. Fleischmann, P. Hendra, and A. McQuillan, "Raman spectra of pyridine adsorbed at a silver electrode," *Chem. Phys. Lett.* **26**, 163–166 (1974).

[79] M. G. Albrecht and J. A. Creighton, "Anomalously intense Raman spectra of pyridine at a silver electrode," *J. Am. Chem. Soc.* **99**, 5215–5217 (1977).

[80] D. L. Jeanmaire and R. P. Van Duyne, "Surface Raman spectroelectrochemistry: Part I. Heterocyclic, aromatic, and aliphatic amines adsorbed on the anodized silver electrode," *J. Electroanal. Chem.* **84**, 1–20 (1977).

[81] K. Kneipp, H. Kneipp, I. Itzkan, R. R. Dasari, and M. S. Feld, "Ultrasensitive Chemical Analysis by Raman Spectroscopy," *Chem. Rev.* **99**, 2957–2976 (1999).

[82] P. L. Stiles, J. A. Dieringer, N. C. Shah, and R. P. Van Duyne, "Surface-enhanced Raman spectroscopy," *Annu. Rev. Anal. Chem.* **1**, 601–626 (2008).

[83] J. P. Camden, J. A. Dieringer, Y. Wang, D. J. Masiello, L. D. Marks, G. C. Schatz, and R. P. Van Duyne, "Probing the structure of single-molecule surface-enhanced Raman scattering hot spots," *J. Am. Chem. Soc.* **130**, 12616–12617 (2008).

[84] B. Sharma, R. R. Frontiera, A.-I. Henry, E. Ringe, and R. P. Van Duyne, "SERS: Materials, applications, and the future," *Mater. Today* **15**, 16–25 (2012).

[85] T. R. Jensen, M. D. Malinsky, C. L. Haynes, and R. P. Van Duyne, "Nanosphere lithography: Tunable localized surface plasmon resonance spectra of silver nanoparticles," *J. Phys. Chem. B* **104**, 10549–10556 (2000).

[86] K. Li, M. I. Stockman, and D. J. Bergman, "Self-similar chain of metal nanospheres as an efficient nanolens," *Phys. Rev. Lett.* **91**, 227402 (2003).

[87] J. Kneipp, X. Li, M. Sherwood, U. Panne, H. Kneipp, M. I. Stockman, and K. Kneipp, "Gold nanolenses generated by laser ablation-efficient enhancing structure for surface enhanced Raman scattering analytics and sensing," *Anal. Chem.* **80**, 4247–4251 (2008).

[88] A. Shiohara, Y. Wang, and L. M. Liz-Marzan, "Recent approaches toward creation of hot spots for SERS detection," *J. Photochem. Photobio. C* **21**, 2–25 (2014).

[89] M. I. Stockman, "Nanoplasmonics fundamentals and surface-enhanced Raman scattering as a physical phenomenon," in *Recent Developments in Plasmon-Supported Raman Spectroscopy*, K. Kneipp, Y. Ozaki, and Z.-Q. Tian, eds. (World Scientific, 2018), pp. 1–32.

[90] K. Kneipp, Y. Wang, H. Kneipp, L. T. Perelman, I. Itzkan, R. R. Dasari, and M. S. Feld, "Single molecule detection using surface-enhanced Raman scattering (SERS)," *Phys. Rev. Lett.* **78**, 1667–1670 (1997).

[91] S. Nie and S. R. Emory, "Probing single molecules and single nanoparticles by surface-enhanced Raman scattering," *Science* **275**, 1102–1106 (1997).

[92] R. M. Stöckle, Y. D. Suh, V. Deckert, and R. Zenobi, "Nanoscale chemical analysis by tip-enhanced Raman spectroscopy," *Chem. Phys. Lett.* **318**, 131–136 (2000).

[93] T. Deckert-Gaudig, A. Taguchi, S. Kawata, and V. Deckert, "Tip-enhanced Raman spectroscopy – from early developments to recent advances," *Chem. Soc. Rev.* **46**, 4077–4110 (2017).

[94] A. Sengupta, M. Mujacic, and E. James Davis, "Detection of bacteria by surface-enhanced Raman spectroscopy," *Anal. Bioanal. Chem.* **386**, 1379–1386 (2006).

[95] R. Weiss, M. Palatinszky, M. Wagner, R. Niessner, M. Elsner, M. Seidel, and N. P. Ivleva, "Surface-enhanced Raman spectroscopy of microorganisms: Limitations and applicability on the single-cell level," *Analyst* **144**, 943–953 (2019).

[96] C. N. Kotanen, L. Martinez, R. Alvarez, and J. W. Simecek, "Surface enhanced Raman scattering spectroscopy for detection and identification of microbial pathogens isolated from human serum," *Sens. Bio-Sens. Res.* **8**, 20–26 (2016).

[97] X. Li, G. Chen, L. Yang, Z. Jin, and J. Liu, "Multifunctional Au-coated TiO_2 nanotube arrays as recyclable SERS substrates for multifold organic pollutants detection," *Adv. Funct. Mater.* **20**, 2815–2824 (2010).

[98] X. Zhang, N. Wang, R. Liu, X. Wang, Y. Zhu, and J. Zhang, "SERS and the photo-catalytic performance of Ag/TiO_2/graphene composites," *Opt. Mater. Express* **8**, 704–717 (2018).

[99] R. Pelton, "Bioactive paper provides a low-cost platform for diagnostics," *TrAC Trends in Analytical Chemistry* **28**, 925–942 (2009).

[100] A. Määttänen, D. Fors, S. Wang, D. Valtakari, P. Ihalainen, and J. Peltonen, "Paper-based planar reaction arrays for printed diagnostics," *Sens. Actuat. B Chem.* **160**, 1404–1412 (2011).

[101] C. H. Lee, L. Tian, and S. Singamaneni, "Paper-based SERS swab for rapid trace detection on real-world surfaces," *ACS Appl. Mater. Inter.* **2**, 3429–3435 (2010).

[102] Y. H. Ngo, W. L. Then, W. Shen, and G. Garnier, "Gold nanoparticles paper as a SERS bio-diagnostic platform," *J. Coll. Interface Sci.* **409**, 59–65 (2013).

[103] M.-L. Cheng, B.-C. Tsai, and J. Yang, "Silver nanoparticle-treated filter paper as a highly sensitive surface-enhanced Raman scattering (SERS) substrate for detection of tyrosine in aqueous solution," *Anal. Chim. Acta* **708**, 89–96 (2011).

[104] S.-W. Hu, S. Qiao, J.-B. Pan, B. Kang, J.-J. Xu, and H.-Y. Chen, "A paper-based SERS test strip for quantitative detection of Mucin-1 in whole blood," *Talanta* **179**, 9–14 (2018).

[105] P. Reokrungruang, I. Chatnuntawech, T. Dharakul, and S. Bamrungsap, "A simple paper-based surface enhanced Raman scattering (SERS) platform and magnetic separation for cancer screening," *Sens. Actuat. B Chem.* **285**, 462–469 (2019).

[106] W. Wei and Q. Huang, "Rapid fabrication of silver nanoparticle-coated filter paper as SERS substrate for low-abundance molecules detection," *Spectrochim. Acta A* **179**, 211–215 (2017).

[107] W. W. Yu and I. M. White, "Inkjet printed surface enhanced Raman spectroscopy array on cellulose paper," *Anal. Chem.* **82**, 9626–9630 (2010).

[108] G. Weng, Y. Yang, J. Zhao, J. Zhu, J. Li, and J. Zhao, "Preparation and SERS performance of Au NP/paper strips based on inkjet printing and seed mediated growth: The effect of silver ions," *Solid State Commun.* **272**, 67–73 (2018).

[109] M. B. Ross, M. J. Ashley, A. L. Schmucker, S. Singamaneni, R. R. Naik, G. C. Schatz, and C. A. Mirkin, "Structure–function relationships for surface-enhanced Raman spectroscopy-active plasmonic paper," *J Phys. Chem. C* **120**, 20789–20797 (2016).

[110] K. Oh, M. Lee, H. Youn, D. Jeong, and H. Lee, "Paper-based chemical detecting sensors for surface-enhanced Raman scattering," in *Advances in Pulp and Paper Research*, W. Batchelor and D. Söderberg, eds. (Trans. of the XVIth Fund. Res. Symp. Oxford, Oxford, 2017), pp. 751–773.

[111] M. Lee, K. Oh, H.-K. Choi, S. G. Lee, H. J. Youn, H. L. Lee, and D. H. Jeong, "Subnanomolar sensitivity of filter paper-based SERS sensor for pesticide detection by hydrophobicity change of paper surface," *ACS Sensors* **3**, 151–159 (2018).

[112] K. Oh, M. Lee, S. G. Lee, D. H. Jung, and H. L. Lee, "Cellulose nanofibrils coated paper substrate to detect trace molecules using surface-enhanced Raman scattering," *Cellulose* **25**, 3339–3350 (2018).

[113] D. Yan, L. Qiu, M. Xue, Z. Meng, and Y. Wang, "A flexible surface-enhanced Raman substrates based on cellulose photonic crystal/Ag-nanoparticles composite," *Mater. Design* **165**, 107601 (2019).

[114] A. T. Vicente, A. Araújo, M. J. Mendes, D. Nunes, M. J. Oliveira, O. Sanchez-Sobrado, M. P. Ferreira, H. Águas, E. Fortunato, and R. Martins, "Multifunctional cellulose-paper for light harvesting and smart sensing applications," *J. Mater. Chem. C* **6**, 3143–3181 (2018).

[115] A. Emeline, V. Kuznetsov, V. Ryabchuk, and N. Serpone, "Heterogeneous photocatalysis: Basic approaches and terminology," in *New and Future Developments in Catalysis*, S. L. Suib, ed. (Elsevier, Amsterdam, 2013), pp. 1–47.

[116] E. Keidel, "Die Beeinflussung der Lichtechtheit von Teerfarblacken durch Titanweiss [Influence of titanium white on the fastness to light of coal-tar days]," *Farben-Zeitung* **34**, 1242—1243 (1929).

[117] C. F. Goodeve and J. A. Kitchener, "Photosensitisation by titanium dioxide," *Trans. Faraday Soc.* **34**, 570–579 (1938).

[118] S.-L. Hwang, P. Shen, H.-T. Chu, and T.-F. Yui, "Nanometer-size α-PbO_2-type TiO_2 in garnet: A thermobarometer for ultrahigh-pressure metamorphism," *Science* **288**, 321–324 (2000).

[119] Z. Li, S. Cong, and Y. Xu, "Brookite vs anatase TiO_2 in the photocatalytic activity for organic degradation in water," *ACS Catal.* **4**, 3273–3280 (2014).

[120] J. Zhang, P. Zhou, J. Liu, and J. Yu, "New understanding of the difference of photocatalytic activity among anatase, rutile and brookite TiO_2," *Phys. Chem. Chem. Phys.* **16**, 20382–20386 (2014).

[121] O. A. Krysiak, P. J. Barczuk, K. Bienkowski, T. Wojciechowski, and J. Augustynski, "The photocatalytic activity of rutile and anatase TiO_2 electrodes modified with plasmonic metal nanoparticles followed by photoelectrochemical measurements," *Catal. Today* **321–322**, 52–58 (2019).

[122] M. Aromaa, A. Arffman, H. Suhonen, J. Haapanen, J. Keskinen, M. Honkanen, J.-P. Nikkanen, E. Levänen, M. E. Messing, K. Deppert, H. Teisala, M. Tuominen, J. Kuusipalo, M. Stepien, J. J. Saarinen, M. Toivakka, and J. M. Mäkelä, "Atmospheric synthesis of superhydrophobic TiO_2 nanoparticle deposits in a single step using liquid flame spray," *J. Aerosol Sci.* **52**, 57–68 (2012).

[123] R. Wang, K. Hashimoto, A. Fujishima, M. Chikuni, E. Kojima, A. Kitamura, M. Shimohigoshi, and T. Watanabe, "Light-induced amphiphilic surfaces," *Nature* **388**, 431–432 (197).

[124] C. Wei, W. Y. Lin, Z. Zainal, N. E. Williams, K. Zhu, A. P. Kruzic, R. L. Smith, and K. Rajeshwar, "Bactericidal activity of TiO_2 photocatalyst in aqueous media: Toward a solar-assisted water disinfection system," *Env. Sci. Technol.* **28**, 934–938 (1994).

[125] A. Kubacka, M. S. Diez, D. Rojo, R. Bargiela, S. Ciordia, I. Zapico, J. P. Albar, C. Barbas, V. A. P. Martins dos Santos, M. Fernández-García, and M. Ferrer, "Understanding the antimicrobial mechanism of TiO_2-based nanocomposite films in a pathogenic bacterium," *Sci. Rep.* **4**, 4134 (2014).

[126] H. Ahmad, S. Kamarudin, L. Minggu, and M. Kassim, "Hydrogen from photo-catalytic water splitting process: A review," *Renew. Sust. Energ. Rev.* **43**, 599–610 (2015).

[127] B. A. van Driel, S. R. van der Meer, K. J. van den Berg, and J. Dik, "Determining the presence of photocatalytic titanium white pigments via embedded paint sample staining: A proof of principle," *Stud. Conserv.* **64**, 261–272 (2019).

[128] T. Watanabe, A. Nakajima, R. Wang, M. Minabe, S. Koizumi, A. Fujishima, and K. Hashimoto, "Photocatalytic activity and photoinduced hydrophilicity of titanium dioxide coated glass," *Thin Solid Films* **351**, 260–263 (1999).

[129] M. Miyauchi, N. Kieda, S. Hishita, T. Mitsuhashi, A. Nakajima, T. Watanabe, and K. Hashimoto, "Reversible wettability control of TiO_2 surface by light irradiation," *Surf. Sci.* **511**, 401–407 (2002).

[130] N. Sakai, A. Fujishima, T. Watanabe, and K. Hashimoto, "Quantitative evaluation of the photoinduced hydrophilic conversion properties of TiO_2 thin film surfaces by the reciprocal of contact angle," *J. Phys. Chem. B* **107**, 1028–1035 (2003).

[131] S. Takeda, M. Fukawa, Y. Hayashi, and K. Matsumoto, "Surface OH group governing adsorption properties of metal oxide films," *Thin Solid Films* **339**, 220–224 (1999).

[132] C.-y. Wang, H. Groenzin, and M. J. Shultz, "Comparative study of acetic acid, methanol, and water adsorbed on anatase TiO_2 probed by sum frequency generation spectroscopy," *J. Am. Chem. Soc.* **127**, 9736–9744 (2005).

[133] M. Stepien, J. J. Saarinen, H. Teisala, M. Tuominen, M. Aromaa, J. Kuusipalo, J. M. Mäkelä, and M. Toivakka, "Adjustable wettability of paperboard by liquid flame spray nanoparticle deposition," *Appl. Surf. Sci.* **257**, 1911–1917 (2011).

[134] M. Stepien, J. J. Saarinen, H. Teisala, M. Tuominen, M. Aromaa, J. Haapanen, J. Kuusipalo, J. M. Mäkelä, and M. Toivakka, "ToF-SIMS analysis of UV-Switchable TiO_2-Nanoparticle-Coated Paper Surface," *Langmuir* **29**, 3780–3790 (2013).

[135] M. Stepien, J. J. Saarinen, H. Teisala, M. Tuominen, M. Aromaa, J. Kuusipalo, J. M. Mäkelä, and M. Toivakka, "Surface chemical analysis of photocatalytic wettability conversion of TiO_2 nanoparticle coating," *Surf. Coat. Technol.* **208**, 73–79 (2012).

[136] H. Teisala, M. Tuominen, M. Stepien, J. Haapanen, J. M. Mäkelä, J. J. Saarinen, M. Toivakka, and J. Kuusipalo, "Wettability conversion on the liquid flame spray generated superhydrophobic TiO_2 nanoparticle coating on paper and board by photocatalytic decomposition of spontaneously accumulated carbonaceous overlayer," *Cellulose* **20**, 391–408 (2013).

[137] M. Tuominen, H. Teisala, J. Haapanen, M. Aromaa, J. M. Mäkelä, M. Stepien, J. J. Saarinen, M. Toivakka, and J. Kuusipalo, "Adjustable wetting of liquid flame spray (LFS) TiO_2-nanoparticle coated board: Batch-type versus roll-to-roll stimulation methods," *Nord. Pulp Pap. Res. J.* **29**, 271–279 (2014).

[138] M. Tuominen, H. Teisala, M. Aromaa, M. Stepien, J. M. Mäkelä, J. J. Saarinen, M. Toivakka, and J. Kusipalo, "Creation of superhydrophilic surfaces of paper and board," *J. Adh. Sci. Technol.* **28**, 864–879 (2014).

[139] J. Balajka, M. A. Hines, W. J. I. DeBenedetti, M. Komora, J. Pavelec, M. Schmid, and U. Diebold, "High-affinity adsorption leads to molecularly ordered interfaces on TiO_2 in air and solution," *Science* **361**, 786–789 (2018).

[140] D. Hunter, *Papermaking - The History and Technique of an Ancient Craft* (Dover, New York, 1978).

[141] E. D. Abrahams, *A Competitive Assessment of the U.S. Paper Machinery Industry* (U.S. Department of Commerce, Washington D.C., 1989).

[142] S.-E. Åström, "The transatlantic tar trade," *Scandinavian Econ. Hist. Rev.* **12**, 86–90 (1964).

[143] Finnish Forest Industries, "Statistics 2019," https://www.forestindustries.fi/statistics/forest-industry/ (6.2.2020).

[144] R. Farnood, "Review: Optical properties of paper: Theory and practice," in *Advances in Pulp and Paper Research*, S. I'Anson, ed. (Trans. of the XIVth Fund. Res. Symp. Oxford, Oxford, 2009), pp. 273–352.

[145] J. Paltakari, "Pigment Coating and Surface Sizing of Paper," in *Papermaking Science and Technolgogy*, E. Lehtinen, H. Paulapuro, and J. Gullichsen, eds. (Paperi ja Puu, Espoo, 2009).

[146] B. T. Hallam, A. G. Hiorns, and P. Vukusic, "Developing optical efficiency through optimized coating structure: Biomimetic inspiration from white beetles," *Appl. Opt.* **48**, 3243–3249 (2009).

[147] C. L. Levy, G. P. Matthews, G. M. Laudone, C. M. Gribble, A. Turner, C. J. Ridgway, D. E. Gerard, J. Schoelkopf, and P. A. C. Gane, "Diffusion and tortuosity in porous functionalized calcium carbonate," *Ind. Eng. Chem. Res.* **54**, 9938–9947 (2015).

[148] M. Lundin Johnson, D. Noreland, P. Gane, J. Schoelkopf, C. Ridgway, and A. Millqvist Fureby, "Porous calcium carbonate as a carrier material to increase the dissolution rate of poorly soluble flavouring compounds," *Food Funct.* **8**, 1627–1640 (2017).

[149] U. Zschieschang, T. Yamamoto, K. Takimiya, H. Kuwabara, M. Ikeda, T. Sekitani, T. Someya, and H. Klauk, "Organic electronics on banknotes," *Adv. Mater.* **23**, 654–658 (2011).

[150] M. C. Barr, J. A. Rowehl, R. R. Lunt, J. Xu, A. Wang, C. M. Boyce, S. G. Im, V. Bulovic, and K. K. Gleason, "Direct monolithic integration of organic photovoltaic circuits on unmodified paper," *Adv. Mater.* **23**, 3500–3505 (2011).

[151] A. Hübler, B. Trnovec, T. Zillger, M. Ali, N. Wetzold, M. Mingebach, A. Wagenpfahl, C. Deibel, and V. Dyakonov, "Printed paper photovoltaic cells," *Adv. Energy Mater.* **1**, 1018–1022 (2011).

[152] F. Brunetti, A. Operamolla, S. Castro-Hermosa, G. Lucarelli, V. Manca, G. M. Farinola, and T. M. Brown, "Printed solar cells and energy storage devices on paper substrates," *Adv. Funct. Mater.* **29**, 1806798 (2019).

[153] M. Berggren, D. Nilsson, and N. D. Robinson, "Organic materials for printed electronics," *Nat. Mater.* **6**, 3–5 (2007).

[154] M. Irimia-Vladu, E. D. Glowacki, G. Voss, S. Bauer, and N. S. Sariciftci, "Green and biodegradable electronics," *Mater. Today* **15**, 340–346 (2012).

[155] R. Bollström, A. Määttänen, D. Tobjörk, P. Ihalainen, N. Kaihovirta, R. Österbacka, J. Peltonen, and M. Toivakka, "A multilayer coated fiber-based substrate suitable for printed functionality," *Org. Electron.* **10**, 1020–1023 (2009).

[156] D. Tobjörk and R. Österbacka, "Paper electronics," *Adv. Mater.* **23**, 1935–1961 (2011).

[157] R. D. Deegan, O. Bakajin, T. F. Dupont, G. Huber, S. R. Nagel, and T. A. Witten, "Capillary flow as the cause of ring stains from dried liquid drops," *Nature* **389**, 827–829 (1997).

[158] A. R. Parker and C. R. Lawrence, "Water capture by a desert beetle," *Nature* **414**, 33–34 (2001).

[159] R. B. Suter, G. E. Stratton, and P. R. Miller, "Taxonomic variation among spiders in the ability to repel water: Surface adhesion and hair density," *J. Arachnol.* **32**, 11–21 (2004).

[160] W. Barthlott and C. Neinhuis, "Purity of the sacred lotus, or escape from contamination in biological surfaces," *Planta* **202**, 1–8 (1997).

[161] C. Neinhuis and W. Barthlott, "Characterization and distribution of water-repellent, self-cleaning plant surfaces," *Ann. Bot.* **79**, 667–677 (1997).

[162] T. Nishino, M. Meguro, K. Nakamae, M. Matsushita, and Y. Ueda, "The lowest surface free energy based on -CF_3 alignment," *Langmuir* **15**, 4321–4323 (1999).

[163] T. Young, "An essay on the cohesion of fluids," *Philos. Tr. R. Soc. Lond.* **95**, 65–87 (1805).

[164] T. Qian, X.-P. Wang, and P. Sheng, "Hydrodynamic slip boundary condition at chemically patterned surfaces: A continuum deduction from molecular dynamics," *Phys. Rev. E* **72**, 022501 (2005).

[165] D. Quéré, "Rough ideas on wetting," *Physica A* **313**, 32–46 (2002).

[166] L. Gao and T. J. McCarthy, "A perfectly hydrophobic surface (θ_A/θ_R = 180°/180°)," *J. Am. Chem. Soc.* **128**, 9052–9053 (2006).

[167] J. C. Maxwell, "Capillary action," in *Encyclopedia Britannica* (A & C Black, London, 1875), pp. 566.

[168] R. W. Wenzel, "Resistance of solid surfaces to wetting by water," *Ind. Eng. Chem.* **28**, 988–994 (1936).

[169] A. B. D. Cassie and S. Baxter, "Wettability of porous surfaces," *Trans. Faraday Soc.* **40**, 546–551 (1944).

[170] J. Bico, C. Marzolin, and D. Quéré, "Pearl drops," *Europhys. Lett.* **47**, 220–226 (1999).

[171] T. Onda, S. Shibuichi, N. Satoh, and K. Tsujii, "Super-water-repellent fractal surfaces," *Langmuir* **12**, 2125–2127 (1996).

[172] S. Shibuichi, T. Onda, N. Satoh, and K. Tsujii, "Super water-repellent surfaces resulting from fractal structure," *J. Phys. Chem.* **100**, 19512–19517 (1996).

[173] L. Liu and W. Shen, "Forced wetting and dewetting of liquids on solid surfaces and their roles in offset printing," *Colloid Interface A* **316**, 62–69 (2008).

[174] T. D. Blake, J.-C. Fernandez-Toledano, G. Doyen, and J. De Coninck , "Forced wetting and hydrodynamic assist," *Phys. Fluids* **27**, 112101 (2015).

[175] T.-S. Wong, S. H. Kang, S. K. Y. Tang, E. J. Smythe, B. D. Hatton, A. Grinthal, and J. Aizenberg, "Bioinspired self-repairing slippery surfaces with pressure-stable omniphobicity," *Nature* **477**, 443–447 (2011).

[176] M. Tuominen, H. Teisala, J. Haapanen, J. M. Mäkelä, M. Honkanen, M. Vippola, S. Bardage, M. E. Wålinder, and A. Swerin, "Superamphiphobic overhang structured coating on a biobased material," *Appl. Surf. Sci.* **389**, 135–143 (2016).

[177] H. Teisala, F. Geyer, J. Haapanen, P. Juuti, J. M. Mäkelä, D. Vollmer, and H.-J. Butt, "Ultrafast processing of hierarchical nanotexture for a transparent superamphiphobic coating with extremely low roll-off angle and high impalement pressure," *Adv. Mater.* **30**, 1706529 (2018).

[178] G. Heydari, M. Sedighi Moghaddam, M. Tuominen, M. Fielden, J. Haapanen, J. M. Mäkelä, and P. M. Claesson, "Wetting hysteresis induced by temperature changes: Supercooled water on hydrophobic surfaces," *J. Coll. Interface Sci.* **468**, 21–33 (2016).

[179] H. Niemelä-Anttonen, H. Koivuluoto, M. Tuominen, H. Teisala, P. Juuti, J. Haapanen, J. Harra, C. Stenroos, J. Lahti, J. Kuusipalo, J. M. Mäkelä, and P. Vuoristo, "Icephobicity of slippery liquid infused porous surfaces under multiple freeze–thaw and ice accretion–detachment cycles," *Adv. Mater. Interf.* **5**, 1800828 (2018).

[180] M. Stepien, G. Chinga-Carrasco, J. J. Saarinen, H. Teisala, M. Tuominen, M. Aromaa, J. Haapanen, J. Kuusipalo, J. M. Mäkelä, and M. Toivakka, "Wear resistance of nanoparticle coatings on paperboard," *Wear* **307**, 112–118 (2013).

[181] F. Temerov, L. Ammosova, J. Haapanen, J. M. Mäkelä, M. Suvanto, and J. J. Saarinen, "Protective stainless steel micropillars for enhanced photocatalytic activity of TiO_2 nanoparticles during wear," *Surf. Coat. Technol.* **381**, 125201 (2020).

[182] D. Wang, Q. Sun, M. J. Hokkanen, C. Zhang, F.-Y. Lin, Q. Liu, S.-P. Zhu, T. Zhou, Q. Chang, B. He, Q. Zhou, L. Chen, Z. Wang, R. H. A. Ras, and X. Deng, "Design of robust superhydrophobic surfaces," *Nature* **582**, 55–59 (2020).

[183] B. Bhushan and M. Nosonovsky, *Rose Petal Effect* (Springer Netherlands, Dordrecht, 2012), pp. 2265–2272.

[184] S. Šikalo, C. Tropea, and E. Ganic, "Dynamic wetting angle of a spreading droplet," *Exp. Therm. Fluid Sci.* **29**, 795–802 (2005).

[185] S. C. Terry, J. H. Jerman, and J. B. Angell, "A gas chromatographic air analyzer fabricated on a silicon wafer," *IEEE Trans. Electr. Dev.* **26**, 1880–1886 (1979).

[186] S. Ma, T. W. Murphy, and C. Lu, "Microfluidics for genome-wide studies involving next generation sequencing," *Biomicrofluidics* **11**, 021501 (2017).

[187] A. W. Martinez, S. T. Phillips, G. M. Whitesides, and E. Carrilho, "Diagnostics for the developing world: microfluidic paper-based analytical devices," *Anal. Chem.* **82**, 3–10 (2010).

[188] F. Costantini, C. Sberna, G. Petrucci, C. Manetti, G. de Cesare, A. Nascetti, and D. Caputo, "Lab-on-chip system combining a microfluidic-ELISA with an array of amorphous silicon photosensors for the detection of celiac disease epitopes," *Sens. Bio-Sens. Res.* **6**, 51–58 (2015).

[189] N. Convery and N. Gadegaard, "30 years of microfluidics," *Micro Nano Eng.* **2**, 76–91 (2019).

[190] R. H. Müller and D. L. Clegg, "Automatic paper chromatography," *Anal. Chem.* **21**, 1123–1125 (1949).

[191] A. W. Martinez, S. T. Phillips, M. J. Butte, and G. M. Whitesides, "Patterned paper as a platform for inexpensive, low-volume, portable bioassays," *Angew. Chem. Int. Ed.* **46**, 1318–1320 (2007).

[192] A. W. Martinez, S. T. Phillips, and G. M. Whitesides, "Three-dimensional microfluidic devices fabricated in layered paper and tape," *Proc. Nat. Acad. Sci.* **105**, 19606–19611 (2008).

[193] G. G. Morbioli, T. Mazzu-Nascimento, A. M. Stockton, and E. Carrilho, "Technical aspects and challenges of colorimetric detection with microfluidic paper-based analytical devices (μPADs) - A review," *Anal. Chim. Acta* **970**, 1–22 (2017).

[194] E. Rosqvist, E. Niemelä, J. Frisk, H. Öblom, R. Koppolu, H. Abdelkader, D. Soto Véliz, M. Mennillo, A. P. Venu, P. Ihalainen, M. Aubert, N. Sandler, C.-E. Wilén, M. Toivakka, J. E. Eriksson, R. Österbacka, and J. Peltonen, "A low-cost paper-based platform for fast and reliable screening of cellular interactions with materials," *J. Mater. Chem. B* **8**, 1146–1156 (2020).

[195] E. Jutila, R. Koivunen, I. Kiiski, R. Bollström, T. Sikanen, and P. Gane, "Microfluidic lateral flow cytochrome P450 assay on a novel printed functionalized calcium carbonate-based platform for rapid screening of human xenobiotic metabolism," *Adv. Funct. Mater.* **28**, 1802793 (2018).

[196] E. Jutila, R. Koivunen, R. Bollström, and P. Gane, "Fully inkjet-printed glucose assay fabricated on highly porous pigment coating," *Microfluid Nanofluid* **24**, 40 (2020).

[197] J. Songok, M. Tuominen, H. Teisala, J. Haapanen, J. Mäkelä, J. Kuusipalo, and M. Toivakka, "Paper-based microfluidics: Fabrication technique and dynamics of capillary-driven surface flow," *ACS Appl. Mater. Inter.* **6**, 20060–20066 (2014).

[198] J. Songok and M. Toivakka, "Controlling capillary-driven surface flow on a paper-based microfluidic channel," *Microfluid. Nanofluid.* **20**, 63 (2016).

[199] A. K. Gnanappa, D. P. Papageorgiou, E. Gogolides, A. Tserepi, A. G. Papathanasiou, and A. G. Boudouvis, "Hierarchical, plasma nanotextured, robust superamphiphobic polymeric surfaces structurally stabilized through a wetting–drying cycle," *Plasma Process. Polym.* **9**, 304–315 (2012).

[200] U. L. Opara, O. J. Caleb, and Z. A. Belay, "Modified atmosphere packaging for food preservation," in *Food Quality and Shelf Life*, C. M. Galanakis, ed. (Academic Press, 2019), pp. 235–259.

[201] Nadia El-Hage Scialabba *et al.*, *Food wastage footprint: Impacts on natural resources* (Food and Agriculture Organization of the United Nations (FAO), New York, 2013).

[202] C. Smith DeWaal, "Safe food from a consumer perspective," *Food Control* **14**, 75–79 (2003).

[203] C. A. Phillips, "Review: Modified atmosphere packaging and its effects on the microbiological quality and safety of produce," *Int. J. Food Sci. Technol.* **31**, 463–479 (1996).

[204] A. L. Brody, "A perspective on MAP products in North America and Western Europe," in *Principles of modified atmosphere and sous-vide packaging*, J. M. Farber and K. L. Dodds, eds. (Technomic, Lancaster, 1995), pp. 13–36.

[205] *Modified Atmosphere Packaging Market - Growth, Trends, and Forecast (2020–2025)* (Mordor Intelligence, 2019).

[206] D. R. Kauffman, C. M. Shade, H. Uh, S. Petoud, and A. Star, "Decorated carbon nanotubes with unique oxygen sensitivity," *Nat. Chem.* **1**, 500–506 (2009).

[207] Y. Z. Lam and J. K. Atkinson, "Screen-printed transcutaneous oxygen sensor employing polymer electrolytes," *Med. Biol. Eng. Comput.* **41**, 456–463 (2003).

[208] S.-K. Lee, A. Mills, and A. Lepre, "An intelligence ink for oxygen," *Chem. Commun.* 1912–1913 (2004).

[209] A. Mills, "Oxygen indicators and intelligent inks for packaging food," *Chem. Soc. Rev.* **34**, 1003–1011 (2005).

[210] S.-K. Lee and A. Mills, "Novel photochemistry of leuco-Methylene Blue," *Chem. Commun.* 2366–2367 (2003).

[211] K. Lawrie, A. Mills, and D. Hazafy, "Simple inkjet-printed, UV-activated oxygen indicator," *Sens. Actuat. B Chem.* **176**, 1154–1159 (2013).

[212] J. Moulder, W. Stickle, P. Sobol, and K. Bomben, *Handbook of X-ray Photoelectron Spectroscopy*, 2nd edition ed. (Perkin-Elmer Corp., 1992).

[213] J. Végh, "The Shirley background revised," *J. Electron. Spectrosc.* **151**, 159–164 (2006).

[214] R. P. Van Duyne, D. L. Jeanmaire, and D. F. Shriver, "Mode-locked laser Raman spectroscopy. New technique for the rejection of interfering background luminescence signals," *Anal. Chem.* **46**, 213–222 (1974).

[215] P. Matousek, M. Towrie, C. Ma, W. M. Kwok, D. Phillips, W. T. Toner, and A. W. Parker, "Fluorescence suppression in resonance Raman spectroscopy using a high-performance picosecond Kerr gate," *J. Raman Spectrosc.* **32**, 983–988 (2001).

[216] J. Kostamovaara, J. Tenhunen, M. Kögler, I. Nissinen, J. Nissinen, and P. Keränen, "Fluorescence suppression in Raman spectroscopy using a time-gated CMOS SPAD," *Opt. Express* **21**, 31632–31645 (2013).

[217] C. R. Barmore and C. Bull, "Method of detecting the permeability of an object to oxygen," *US Patent* 5 483 819 (1996).

[218] T. A. Blinka, C. Bull, C. R. Barmore, and D. V. Speer, "Method of detecting the permeability of an object to oxygen," *US Patent* 5 583 047 (1996).

[219] G. Silva and L. C. Di Serio, "The sixth wave of innovation: Are we ready?," *RAI Revista de Administração e Inovação* **13**, 128–134 (2016).

[220] W. Steffen, K. Richardson, J. Rockström, S. E. Cornell, I. Fetzer, E. M. Bennett, R. Biggs, S. R. Carpenter, W. de Vries, C. A. de Wit, C. Folke, D. Gerten, J. Heinke, G. M. Mace, L. M. Persson, V. Ramanathan, B. Reyers, and S. Sörlin, "Planetary boundaries: Guiding human development on a changing planet," *Science* **347**, 1259855 (2015).

Jarkko J. Saarinen

Nanophotonics on Paper Platform

Nanotechnology and nanophotonics were combined in this work with sustainable materials. Three nanophotonic applications based on printed and coated functionality were developed on natural fibre based substrates. Demands for sustainability have grown significantly in recent years with growing population and emerging environmental issues. Nanotechnology is an ideal tool for promoting sustainability: with less material and energy consumption one can generate the same or even enhanced properties. Combining such nanoscale structures with renewable materials provides a double advantage compared to the traditional solutions.